AN INTEGRATED COMPUTATIONAL AND EXPERIMENTAL APPROACH FOR SELECTION OF AN OPTIMUM BULLET PROOF ARMOR

SUBMITTED BY:

Ahmed Raza Tariq
2011-NUST-MS Phd-02

Submitted to the Department of Mechanical Engineering in Fulfillment of the Requirements for the Degree of

MASTER OF SCIENCE
In
MECHANICAL ENGINEERING

THESIS SUPERVISOR

DR HASAN AFTAB SAEED

COLLEGE OF ELECTRICAL AND MECHANICAL ENGINEERING

NATIONAL UNIVERSITY OF SCIENCES AND TECHNOLOGY

2015

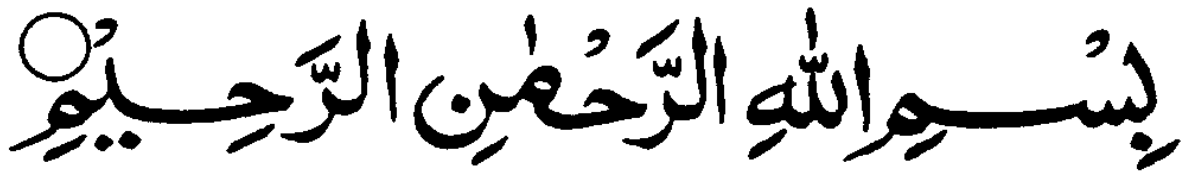

In the name of Allah, the most Beneficent and the most Merciful

Abstract

During recent times, armouring industry has significantly flourished and has also seen large financial influx to develop and test new armours. Experimental set up for ballistic studies is costly followed by an experimental procedure, which is tardy and complex with a lot of sensors and cutting edge imaging technology. Also the experimental data which is mostly reliable does not capture all the required parameters. Substantial amount of research is being carried out to devise numerical and analytical models to accurately predict the ballistic performance of new armour designs and materials.

This thesis presents a study of the ballistic performance of monolithic and multi layered target sheets against blunt and conical nose projectiles. Impact phenomenon including Adiabatic Shear Localization, Thermal Plastic Instabilities and High gradient of stresses have been modeled using FEM based explicit analysis solver. Appropriate strength, failure and shockwave models have been used both for brittle and ductile materials. Selected targets were tested against blunt and conical projectile moving in a velocity range of 200-500 m/s. Result from impact simulations have been compared with the experimental data and analytical solution findings. By using different grades of metals and ceramic of varying strength and ductility in target shields, the combined effect of ductility and strength on energy dissipation and ballistic resistance has been investigated. Materials namely SiC, Al 7075 & Steel alloys including Weldox 460E & 4340 were investigated as eligible options for a ballistic target. Moreover, dominant failure modes in each case were observed and identified. It has been shown that FEM based simulations with carefully selected material and computational models produce quite comparable results. In the end, a comprehensive stud of seven different target configurations including monolithic and multi-layered option with different materials against a blunt projectile has been presented.

Acknowledgement

Innumerable words of praise and thanks to Allah, the Almighty. Without His Will and Mercy, I would not have been able to accomplish this milestone of my academic career.

I would like to thank my advisors Dr Wasim Akram and Dr Hasan Aftab Saeed who guided me in my research. I would like to thank Dr. Wasim Akram for believing in me and providing me with the much needed moral support and technical guidance required for this work. I would also like to thank my guidance and evaluation committee members Dr Rizwan Saeed Choudhry & Dr. Abdul Waheed Badar for their continuous support and encouragement.

My deepest thank to Mr Shahid Hassan & Mr Munawar Muhammad, who supported me throughout my studies. Thanks to my colleagues at NDC (Waqas Muneer, Shehzad, Zaheer Abbas, Mohsin Khan, Sarfraz Dogar and Ahsan Ali Zaidi).

Special thanks to my mother and father who provided me with all the comfort and resources. I want to thank my brother, Shahzaib Tariq and my sister, Aamna Tariq for their continuous love and support.

Declaration

I hereby declare that I have developed this thesis entirely on the basis of my personal efforts and under the sincere guidance of my supervisor Dr Hasan Aftab Saeed. All the sources used in this thesis have been cited and the contents of this thesis have not been plagiarized. No portion of the work presented in this thesis has been submitted in support of any application for any other degree of qualification to this or any other university or institute of learning.

_____

Ahmed Raza Tariq
2011-NUST-MS Phd-02

Table of Contents

List of Figures

List of Tables

Nomenclature

v_r	Residual Velocity of the Projectile		
v_i	Initial Velocity of the Projectile		
v_{bl}	Ballistic Limit Velocity		
a_0	Coefficient of Approximation		
n	Coefficient of Approximation		
b	Thickness of Shield		
R	Shank Radius of the Projectile		
σ_{ij}	Cauchy Stress Tensor		
A	Initial Yield Stress		
B	Strain hardening Coefficient		
n	Strain Hardening Exponent		
$\tilde{\varepsilon}_p$	Plastic Strain Rate		
$\dot{\varepsilon}_0$	Reference Strain Rate		
C	Strain Rate Coefficient		
T_r	Room Temperature		
T_m	Melting Temperature		
$\boldsymbol{m}$	Thermal Softening Exponent		
ρ	Density		
σ_H	Hydrostatic Stress		
EOS	Equation of State		
Γ	Gruneisen Constant		
σ_{ij}^D	Deviatoric Stress Tensor		
δ_{ij}	Kronecker Delta		
$\boldsymbol{m_p}$	Mass of Projectile		
$\boldsymbol{v_{rpl}}$	Residual plug velocity		
$\boldsymbol{m_{pl}}$	Mass of the plug formed		

CHAPTER-1

1. INTRODUCTION

As Wright and Frank state

"Given a projectile, target and details of the initial geometry, kinematics and materials; determine whether or not the target will be perforated upon impact. If perforated, determine what the residual characteristics of the projectile and target will be, and if not how deep a hole will be made".

1.1 MOTIVATION

Since the dawn of mankind, violence in the form of war, criminal activities including killings and bombings have been an integral part of human nature or society in one form or the other. Mankind have always looked to plan for such actions by building strongholds like castles, bunkers & underground dwellings. Above all, personnel protection and safety has always been a top priority. Throughout the centuries, weapons technology has been immensely improved and now able to hit targets quite accurately far beyond the visual range. As compared to the weapon's technology, armouring wasn't given much thought until the start of First World War. Same old practices and materials were being used. A complete up gradation of armouring techniques was required to counter ever increasing bullet speed and sizes. Seeing this opportunity, special materials are being developed today, with the sole purpose of protection against ballistic impacts. Apart from bullet, shrapnel produced as a result of road side and suicide bombings also account for huge number of deaths. Due to these new kinds of terrorism threats, security forces need to be equipped with best possible armours. Armed and Paramilitary forces are not the only one facing the grave danger of being attacked with fire arms. The government representatives and public figures also need protection from such unforeseen threats. Looking on the statistical data it was gathered that 80-90% of terrorist attacks occur while the victims are travelling by automobiles. Due to this, a number of security officials have lost their lives to suicide bombers and IEDs. Given the current national scenario, readily available security solutions are required. A properly armored vehicle whether it's manned or unmanned can effectively help disarm potential terrorists. It can also provide much required security during movement of troops and patrolling by protecting them against unforeseen circumstances. Researchers working in the field of impact dynamics can play an important role in this regard.

1.2 IMPACT MECHANICS

Research into the field of structural impact dynamics has resulted in a large amount of work published in the literature. Many of these investigations have been carried out on generic

components under idealized impact conditions, i.e. normal impact of moving projectiles against fixed targets. Such idealized scenario can only be observed inside a laboratory. In real life applications, a wide range of different projectile-target configuration exists, and these may differ significantly from generic laboratory investigations. Structural impact dynamics has some features that differentiate it from conventional quasi-static loading conditions. From a physical point of view, inertia effects need to be accounted for in all governing equations. This result in propagating stress wave in the impacting projectile as well as the target, which is clearly a recognition that steady state conditions do not apply to such transient impact events. From a material point of view, the short duration of impact phenomena may introduce strain effects, thermal softening and hydrodynamic material behavior, not observed in quasi-statically loaded materials. Also, from an experimental point of view the high rate of loading involves great challenges, as it is far more difficult both to apply the load and to record the response.

Impact Dynamics has two features which distinguish it from the more conventional disciplines of the classical mechanics of rigid or deformable bodies under quasi-static conditions. The first is the importance of inertia effects which must be considered under in all of the governing equations based upon the fundamental conservation laws of mechanics. The second is the role of stress wave propagation in the analysis of problems and the recognition that most impact events are transient phenomenon where steady state conditions do not exist [1].

Three kinds of approaches are generally used to solve impact problems. First one is an empirical approach based on the experimental data. With the right equipment and experimental setup, most accurate results can be obtained. Although a very realistic approach, extrapolation of problem specific results can be extremely difficult. Second approach is the formulation of ballistic impact models based on the laws of conservation of momentum and energy. These kind of models also incorporate some of the material properties including density, yield and ultimate tensile strengths. Some of these models including the one proposed by Lambert and Jonas are merely based on curve fitting techniques and relate to a specific problem or a set of materials. Third approach to solving such problems is discretization using either Lagrangian or Eulerian schemes. The solution obtained depends specifically on the failure and strength models used and can be very time consuming. Margin of error can be significantly reduced using appropriate modeling parameters and techniques.

Many publications in this area have resulted in conflicting use of several technical terms, which may cause confusion since their meaning not always are obvious. Some of these terms

will be defined here. In modern science, Ballistics deals with the motion, forces and impact of projectiles, especially those discharged from firearms and guns. During the course of work, our main focus will be on studying the terminal ballistics that is the projectile-target interaction during impact. This is the area of most interest with respect to armoring, which may be defined as the structures used for additional strength or strengthening, especially in military defenses. During impact the projectile may penetrate the target in several ways. Backman and Goldsmith (1978) suggested the following definitions

a. Perforation if the projectile passes through the target with a final residual velocity
b. Ricochet if the projectile is deflected from the target without being stopped

Figure 1 depicts the most common failure modes observed when the strength of the projectile exceeds the target strength. These failure modes have been categorized into two generic types depending on the ductility of target.

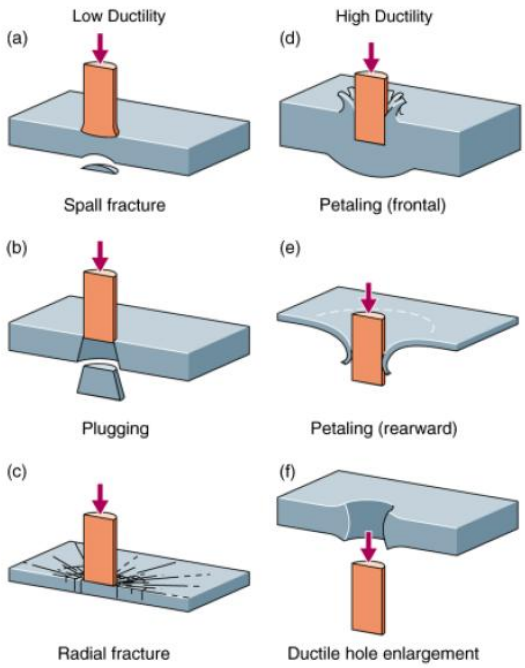

Figure 1 – Common Failure Modes

1.3 LOW DUCTILITY

Low ductility regime has been further classified in to three failure modes depending on the target material, thickness and strength:

a. Spall fracture (Fig-1(a)): This kind of fracture can usually be observed on the back side of the target. Compressive shock wave which emanates from the point of impact is reflected back as a tensile wave from the rear end of the target. Target failure due to spall fracture occurs if the reflected tensile wave has a magnitude greater than the tensile strength of the material.

b. Plugging (Fig-1(b)): Such failure mechanism usually occurs in highly ductile metallic targets. A plug nearly the diameter of projectile is ejected from the rear side of the target. This is due to the formation of high stress shear zones around the circumferential periphery of moving projectile. Temperature of target material inside the shear zone usually approaches its melting temperature. In metals, this is typically referred as Adiabatic shearing.
c. Radial fracture (Fig-1(c)): This is a common failure mode for ceramic targets primarily due to the fact that the tensile strength of ceramics is lower than their compressive strength. Same compressive stress wave, observed during projectile impact in ductile materials, results only this time in a tensile radial stresses.

1.4 HIGH DUCTILITY

High ductility regime can be broadly classified in to two failure modes, based on the target thickness. This category includes highly ductile metals like stainless steel and polymers.

a. Petaling (Figs-1(d) and (e)): Two kinds of petaling can be observed that is: Frontal (Fig-1(d)) and Rear (Fig-1(e)). Frontal petaling is the most common failure mode in soft ductile targets impacted by sharp projectiles. This is due to very high tensile stresses, as the initial stress wave passes through the target. Both radial and circumferential tensile stresses can be observed inside the critical area of penetration. Significant plastic deformation can be observed as the target material flows in front of the impacting projectile. Radial expansion of initial hole formed as a result of material flow after projectile impact produces a petal kind shape in front of the projectile. Now as the target thickness decreases, work required to bend and stretch the target decreases as compared to radial expansion. High bending stresses produced due to projectile impact result in rear petaling of the target. This kind of failure is also termed as dishing.
b. Ductile Hole Enlargement (Fig-1(f)): This kind of failure is most commonly observed in relatively thick targets impacted by sharp nose projectiles including ogival and conical ones. As the projectile impacts the target, kinetic energy of the projectile displaces the adjacent target material to form a hole inside target plate. As the projectile further penetrates the target, radius of initial hole increases. Plugging and ductile hole enlargement are two similar failure modes converting the projectile kinetic energy in to plastic deformation but ductile hole enlargement is dominant, as the target thickness exceeds the projectile diameter.

Ballistic limit velocity "v_{bl}" is the average of maximum projectile velocity which does not penetrate the target and the minimum projectile velocity resulting in complete penetration of

target. In addition to Ballistic limit velocity, Ballistic limit curve is an important measure in structural impact. It gives the residual projectile velocity as a function of initial projectile velocity.

Residual velocity can be calculated from an analytical model proposed by Lambert and Jonas:

$$\hat{v}_{res} = a_0\left(\hat{v}_{imp}^{n} - 1\right)^{1/n}, \hat{v}_{imp} = \frac{v_{imp}}{v_{bl}}, \hat{v}_{res} = \frac{v_{res}}{v_{bl}}, \hat{v}_{imp} > 1 \Rightarrow \quad (1)$$

Where v_{res} and v_{imp} are the residual and initial projectile velocity respectively, a_0 and n are the coefficients of approximation.

Residual projectile velocity when plotted against impact velocity results in the kind of graphs given below. Such graphs are most commonly known as "Ballistic limit curve". It is a proven technique to study the ballistic resistance of a target and also to check the target's performance with the increase in the projectile's impact velocity.

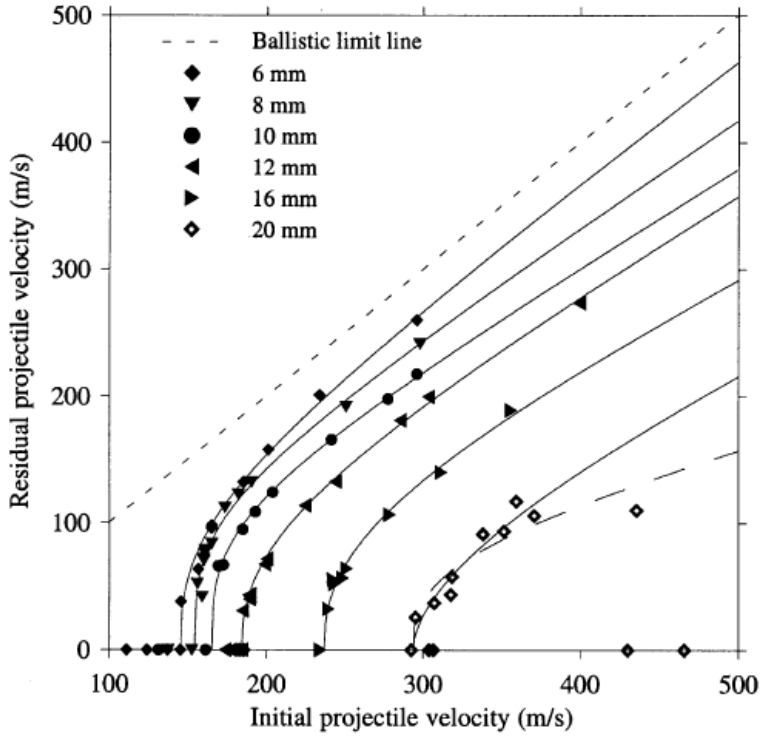

Figure 2 – Ballistic Limit Curve

Above plots present a general picture of the penetration capability of a blunt projectile against targets of varying thickness.

Experimental studies on ballistics can be broadly grouped into three major categories depending on the projectile's impact velocity. The first group includes projectiles with impact velocity"v_i" $\leq 50\ m/s$. This holds for heavy projectiles using a drop hammer or a pneumatic

accelerator. The second group includes projectiles travelling at sub-ordinance to ordnance velocities. These velocities are usually achieved using compressed gas guns to accelerate a projectile of arbitrary mass and shape to an impact velocity of 50-1300 m/s. Most of the research carried out during this thesis is focused on this category of impact velocity. Final category covers the projectiles moving in hyper velocity regime. This is usually achieved by using two-stage light gas guns and low-mass projectiles. This research study will be concentrated in the sub-ordinance velocity regime with a few simulations in ordnance velocity regime. The final aim of this thesis is to reach an optimum armouring solution, while also validating the results of the ballistic experiments using an integrated numerical and analytical approach.

1.5 BALLISTIC TESTING STANDARD

Main objective behind studying ballistic impact phenomenon is the optimization of existing protection techniques. Obviously such protection cannot be offered against all kinds of projectiles. So we have to limit our study based upon the projectile type and velocity. We will work with much simpler geometries to validate our simulation setup and techniques. Most of the research groups have started out with blunt, ogival or conical shaped projectiles. Final selection of optimum armour depends on the ballistic resistance shown against blunt projectile with the initial impact velocities in the range of 200-600 m/s.

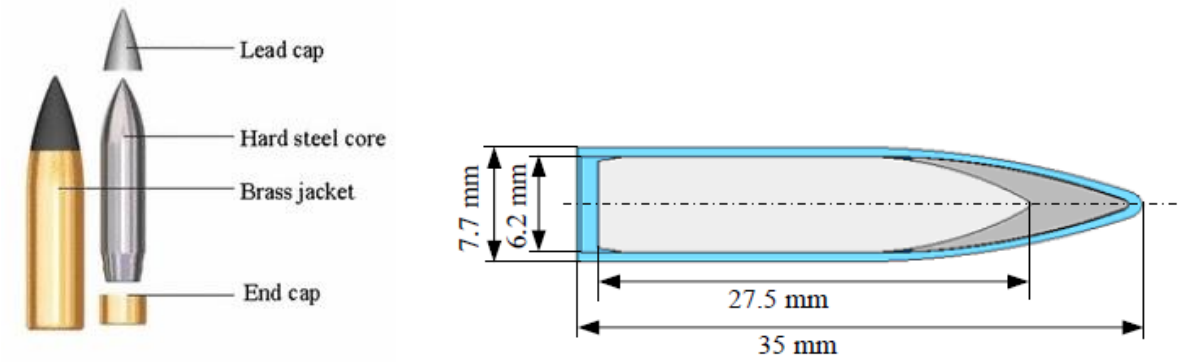

Figure 3 – 7.62 mm (.30 Cal) Projectile

CHAPTER-2

2. LITERATURE REVIEW

Most of the research done by military and industrial research organisations in the field of armouring isn't open for general public access. Still, a lot of experimental data is available in the form of published literature produced in research labs around the globe. Aim of such research studies are extremely varied ranging from the effect of different projectile shapes to the study of ballistic resistance of different target materials and their varying thickness.

2.1 MONOLITHIC METALLIC SHEETS

Borvik et. Al [3,4] was the first group to thoroughly study the ballistic resistance properties of monolithic sheets. Most of their research is based on extensive experimental work. They also did comparative studies of analytical and numerical results for ballistic resistant Weldox 460 E steel targets. Variables studied during testing were the plate thickness (which varied from 6 to 30 mm), projectile nose shape (blunt, conical) and the initial projectile velocity. They concluded that the target becomes sensitive to changes in impact velocity close to the ballistic limit velocity. They showed that the ballistic limit curve jumps to zero residual velocity without showing any prior signs, as the ballistic limit velocity is reached. They also plotted a hypothetical line called ballistic limit line on their plots, which is the ballistic limit velocity of a zero thickness target. Results obtained by Borvik et al. also exhibited that the plug velocity is greater than the projectile's residual velocity.

Borvik also studied the kinetic energy absorbed as the projectile tries to penetrate through the target and showed that the kinetic energy absorbed becomes constant with increasing impact velocity. Also the target deformation decreases with the increase in impact velocity. Opposite scenario was observed with the decrease in impact velocity, where the deformation increases to a maximum up till ballistic limit velocity. Target deformation can be categorized in to two types: Local and Global deformation. Global deformation increased with the decrease in impact velocity while opposite was observed for local deformation which increased with impact velocity. An upward trend in the plastic deformation of projectile was computed with projectile velocity.

Another field of interest in ballistic studies was failure mechanism of a target as described in Introduction. Target's failure was strictly dependent on a range of parameters like projectile shape, its velocity, target thickness and target material. All these penetration mechanisms are summarized by Backman and Goldsmith as radial fracture due to initial stress wave for brittle

materials, compressive stress wave failure, ductile hole enlargement and plugging. Plugging along with ductile hole enlargement was the dominant failure mode for metallic targets.

A close study of plugging and ductile hole enlargement reveals that both failure modes are pretty different as far as the energy absorption is concerned. Plugging using adiabatic shear phenomenon induces high shear stress regions around the edges of projectile. While, ductile hole enlargement pushes the material in front of the projectile and requires more energy to do so as compared to plugging. For relatively thin targets, plugging takes place using localized shear and global bending. Initially, when a projectile hits a thick target, ductile hole enlargement can be observed but as the target thickness in front of the penetrating projectile decreases, perforation mechanism changes to plugging which can dissipate impact energy more quickly. T. Borvik et al. carried out a microscopic analysis of the perforated target sheets and observed heavily deformed shear bands in 10–16 mm thick targets. They also observed transformed adiabatic shear bands in relatively thick taregts.

2.2 MULTILAYERED METALLIC SHEETS

First obvious question in multi-layered targets was, whether there is any advantage in dividing a monolithic target; say a 10 mm thick Weldox sheet into two 5mm plates. Another burning question was either to use spaced plates or simply layered ones. Marom and Bonder used a combined analytical and experimental approach, using a spherical nose projectile to address such issues. They concluded that monolithic targets give higher ballistic resistance as compared to multilayered target when the target sheets are joined together without any space. Opposite was found for spaced shields.

Such evidence even conclusive has been challenged by other researchers in the field of ballistic studies. Radin and Goldsmith proved the opposite for blunt and conical projectiles against multi-layered shields of thickness 1.6-6.4 mm. They proved through experimental results that monolithic targets have higher ballistic resistance against multi-layered targets against all kinds of projectiles. These results were confirmed by Almohandes et al. They did a thorough experimental study for 7.62mm bullets. They used three target configurations: spaced, layered & monolithic with thickness varying from 8-14 mm. Their results were in complete agreement with those of Radin & Goldsmith. They also concluded based on the experimental results that this difference in ballistic resistance of monolithic and layered targets reduces with increasing impact velocity. Alomohandes et al proved on the basis of his experimental work, that in a double layered target, a thicker rear plate resulted in more ballistic resistance as compared to thin rear plate. A downward trend in ballistic resistance is

observed with increase in the number of layers for Multi-layered targets. They also studied multi-layered plates with polyester filled inside the core and concluded that these plates show high ballistic resistance as compared to steel targets with same weight. Liang et al. [2005] proposed an approximate penetration model and validated his model using the experimental results of Almohandes et al. [1996]. They proposed an optimum ratio of front plate's thickness to target's total thickness based on their approximate analytical model. Best results were obtained for thickness ratio of 0.75 and minimum ballistic resistance was observed for thickness ratio equal to 0.5. They also studied the effect of air gap between two plates in double layered targets.

Dey et al. carried out a detailed numerical and experimental analysis of multi-layered steel targets. They observed that ballistic limit velocity of double-layered target is 30% higher than monolithic target for blunt nose projectile. Even with such an extensive amount of research data available, experimental analysis have occasionally resulted in contradictory findings for same projectile-target impact configurations.

Corran et al. concluded that double layered target may provide high ballistic limit velocity, if the target thickness is greater than a specific value. They plotted penetration energy against target thickness for somewhat hemispherical projectiles and observed a sharp twist in the curve at a value of 3.5 mm. Below this value, multi-layered targets did not provide any benefit. This irregular occurrence was due to the change in energy absorption method. Corren at al. also concluded that order of sheets in a target of unequal sheet thickness is critical. They also computed that best thickness combination for front and rear sheet above 3.5 mm could give results comparable to monolithic targets.

Nixdorff concluded that partitioning of a monolithic and homogeneous target into multi layers result in a decrease in target's ballistic limit velocity. He based his findings on a theory published by Awerbuch and Bodner.

Zukas and Scheffler conducted a thorough numerical study of metallic targets. They proposed a parameter $b/2R$ where b and R are target thickness and radius of projectile's shank respectively. They concluded that layering has a very negative effect on ballistic properties of thin $(b/2R) < 1$ and intermediate thickness $3 < (b/2R) < 10$ targets. Also that for a value greater than 10 in case of thick targets, there is no significant change in the residual properties of the projectile as compared to their monolithic equivalent.

Madhu et al. performed extensive experimental work on normal impact of aluminium targets and compared monolithic targets with double and triple layered plates of equal thickness. Authors found out that layering does not improve the ballistic resistance of intermediate

thickness targets. Their results for aluminium and steel targets supported the findings of Zukas & Scheffler. Results obtained for Steel and Aluminium by above mentioned authors targets can be easily extrapolated for other metallic targets.

Steel is a high density material which sometimes overshadows its better ballistic performance. A substantial amount of research, based on numerical and analytical results, has been conducted to study the effect of different metallic options as a combination in multi-layered targets. Zukas also proposed an analytical solution regarding the arrangement of metallic sheets of different materials in a multi-layered target. They sought to optimize the combined effect of ductility and strength on energy dissipation. They proposed that metallic layers should be ordered in increasing order of parameter χ, computed as the ratio of dynamical hardness to density. This placed Aluminium in front of Steel for better ballistic performance. Another new proposal is to replace some of the steel mass from target with relatively less dense ceramic plate which has high compressive strength as well.

2.3 MULTILAYERED SANDWICH CORE WITH CERAMIC PLATES

Another new development has been recently observed in multi-layered targets. According to this, a double-layered target with sandwich core is used. This core is then filled with a optimum material usually ceramic or polymer for better ballistic performance. Idea is to replace high density steel with light weight alternatives without compromising the ballistic performance. Some of the alternatives like ceramic not only reduce target weight but also has its own ballistic resistance properties like interface defeat phenomenon. This specific property of ceramics deforms the projectile dissipating much of its kinetic energy. Plastic deformation through mushrooming is a common occurrence for projectiles impacting against ceramic targets. When this ceramic plate is placed between two metallic plates, its pulverization furthers reduces the kinetic energy of penetrating projectile. Sarva et al. proposed that ballistic efficiency can be increased up to 25% for a 2.5% increase in areal density by sandwiching a ceramic tile between two ductile plates. This confinement on both sides results in increase in the strength of ceramic as published by Deshpande and Evans. Reason behind this revolutionary improvement in the ballistic performance of ceramics is the change of failure mode. Variation in failure mode can be observed in the figure given below. Even after pulverization, ceramic bears much of the impact force.

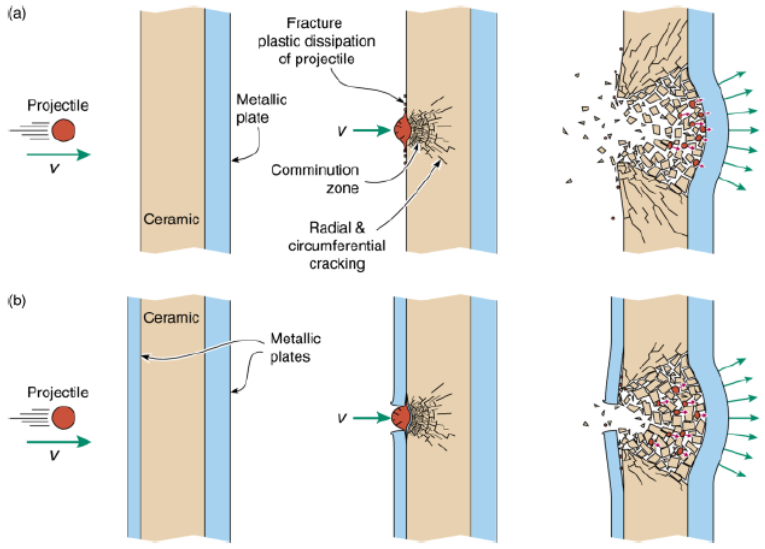

Figure 4 – Sandwich Panels

Christian et al. studied the stainless steel sandwich of pyramidal shaped truss core with the core filled with polyurethane and alumina against spherical projectile. They concluded that polyurethane core does not improve the ballistic limit as compared to monolithic steel target but somehow reduced the kinetic energy of projectile. Reason being that polyurethane fails due to hole enlargement which does not distribute the impact load efficiently. While on the other hand, targets with Alumina inserts perform quite well eroding the impacting projectile at the same time engaging the steel plates to absorb impact energy.

2.4 PROMISING MATERIALS

The work done in plastic deformation of a metal appears largely as heat, and if not conducted away, as in the case of high speed deformation, the temperature rises. In those metals, where the rate of thermal softening exceeds the rate of work hardening, deformation is observed to concentrate in a narrow softened region producing a band of adiabatic shear [1]. Ballistic penetration is a localized phenomenon triggering shock waves and producing exceptionally high strain rates depending upon the velocity of impacting projectile. Adiabatic shear is a deformation mode unique to these high strain rates. In case of metals, ballistic penetration results in large plastic deformation. 95% of this plastic deformation is converted to heat, which result in temperature rise. Adiabatic deformation requires low thermal conductivity and a small deformation time, which makes it one of the most important phenomenon to be modelled in high velocity impact loading cases. Yellup and Woodward [5] produced graph ranking materials in terms of strength to weight ratio and their susceptibility to adiabatic shear. They concluded that adiabatic deformation requires low thermal conductivity and very

small deformation times of the order of milli to micro seconds. Selection of an optimum material with appropriate properties is the key to high ballistic resistance. Ceramics cannot be ignored in this regard. The high strength of ceramics in combination with their low densities enables the design of weight efficient armour systems with high protection capability. A lot of options are available ranging from metallic shields like steel and aluminium to composites including SiC and Boron Carbide. Each material has its own properties like density, yield strength, specific heat etc. Carbides have a high compressive strength as compared to their tensile strength, which can come in handy during projectile penetration. The optimum selection does not depend upon a single metallic/non metallic sheet but a wisely chosen combination of different materials.

CHAPTER-3

3. COMPUTATIONAL MODELING

Projectile impacting a target dissipates its kinetic energy in a fluid flow like process. Projectile after impact tries to create a channel along its path inside the target just like fluid flowing through a constriction. Much of the material loss in case of projectile occurs due to erosion. During this process, shock waves are generated which propagate away from the contact surfaces. At the same time, release waves from the projectile boundaries initiate lateral flow from both projectile and target materials.

A solid on which a deformation is imposed at such an arbitrary rate can accommodate this deformation by six basic modes: Elastic Distortion, Homogenous Plastic Flow, Phase Changes, Nucleation and growth of ductile micro voids, nucleation and growth of brittle micro cracks and nucleation and growth of shear instabilities [8]. A robust and efficient numerical approach is imperative for impact problems since experimental studies usually require high cost and complex setups. Commercial codes like ABAQUS, AutoDyn and LS Dyna have been written to cater for such short duration loadings. The problem in this specific case is the wide range of materials to be modeled starting from ductile to brittle ones. An accurate simulation of projectile impact would require a realistic approach covering difficult problems like Adiabatic Shear Localization, Thermal Plastic Instabilities and High gradient of stresses. Dynamic deformation processes are usually modeled by a decomposed stress tensor. This decomposition results in Deviatoric stress tensor σ_{ij}^{D} and Spherical hydrostat $\sigma_H \delta_{ij}$ categorized as plasticity and pressure terms respectively.

$$\sigma_{ij} = \sigma_{ij}^{D} + \sigma_H \delta_{ij} \rightarrow (2)$$

There are basically five kinds of numerical approaches normally used for solving such problems: Lagrangian, Eulerian, Arbitrary Lagrangian Eulerian (ALE), Smooth Particle Hydrodynamics (SPH) and SFM models. Last two methods can be categorized as an extension of Mesh-Free techniques.

3.1 LAGRANGIAN FORMULATION

In Lagrangian formulation, each individual node of the computational mesh follows the associated material particle during motion. Such codes are conceptually straightforward, and easily handle the boundary conditions at free and contact surfaces between different materials. Its main limitation is its inability to follow large distortions of the computational domain without recourse to frequent remeshing operations.

3.2 EULERIAN FORMULATION

In Eulerian codes the grid is fixed in space, and the continuum moves with respect to this grid. Moreover, the elements are created by connecting the grid points. Subsequently, the Eulerian mesh must be large enough to model existing as well as the future regions where material may flow. Eulerian codes can handle flows with large distortions in a satisfactory manner. But they are inadvertently coupled with relatively inaccurate free surface motion calculations and conditions at material interfaces.

3.3 ARBITRARY LAGRANGIAN EULERIAN FORMULATION

ALE technique was developed to address the inherent issues in Eulerian and Lagrangian schemes and to combine their positive features. In the ALE, the nodes of computational may be moved with the continuum in the normal Lagrangian fashion, or be held fixed in Eulerian manner, or be moved in some arbitrarily specified way to give a continuous rezoning capability. It allows the handling of larger distortions in the continuum by offering the freedom in the movement of computational mesh, while at the same time with more resolution than normally offered by Eulerian techniques.

Since there are no convective terms for the motion of material through a grid as in the Eulerian case, Lagrangian codes require fewer computations per cycle and time histories are easily obtained.

Finite element method (FEM) suffers from a serious mesh distortion problem when used for high velocity impact analyses. This phenomenon introduces numerical difficulties leading to negative volume problem and premature termination of the analysis.

3.4 SMOOTH PARTICLE HYDRODYNAMICS

Fourth one is the Mesh-Free techniques. There is an obvious lack of accuracy on part of mesh based schemes in the treatment of discontinuities that do not coincide with the original mesh edges. Remeshing often used to cater for moving discontinuities can lead to inaccurate results and high computational cost. The objective of these methods is to eliminate at least part of this mesh dependence by constructing the approximation entirely in terms of nodes. One of the widely used mesh free techniques is Smooth particle Hydrodynamics (SPH).

SPH is a mesh free technique that can be applied for non-linear problems with large deformations. It is stated that SPH overcomes the disadvantages of the Lagrangian and Eulerian approaches. In the SPH formulation free moveable points with a fixed mass, called particle, have coherence by means of an interpolation function. A kernel estimate describes the conservation of mass, momentum and energy in terms of interpolation sums. A physical object is then defined by a field of SPH points instead of elements. The problem of this

formulation is the large velocity oscillations in single particles. Other inherent undesirable phenomena associated with standard SPH methods, such as tension instability and unstable execution caused by shockwave, have to dealt with by a combination of remedial measures, e.g., introducing the additional stress method and the artificial viscosity term to mitigate the above two deficiencies respectively [26].

3.5 SFM

Like ALE, a coupled SPH-FEM (SFM) approach was proposed, in which the SPH particles are used in the region of expected large deformation and damages, while the rest of the domain modeled by the Finite Element (FE) mesh.

It is beneficial if SPH is adopted only in severely distorted regions and FEM further away. S. Swaddiwudhipong et al. [26] proposed a coupled smooth particle hydrodynamics and FEM technique to study the perforation of Weldox 460E steel and AA5083-H116 aluminum plates with varying thicknesses and various projectile nose geometries including blunt, conical and ogival noses. The study showed that SFM is able to emulate the same failure mechanisms of the steel and aluminum plates as observed in various experimental investigations for initial impact velocity of 170 m/s and higher.

In elastic-viscoplastic materials, the Cauchy stress tensor σ_{ij} is dependent only on the state of strain. Yield stress changes with increasing plastic deformation and its rate above certain level of stresses. It is possible to use elasto-visco-plasticity coupled with damage constitutive equations and a Finite Element numerical procedure as long as the effects of temperature are represented by proper functions. For the latter, one may use either the expression of yield stress function of the strain rate and the temperature.

3.6 JOHNSON AND COOK STRENGTH MODEL

Johnson and Cook expressed the equivalent stress as a function of plastic strain, strain rate and temperature. It is the easiest model to use, reason being the range of tests available to isolate and establish the static, dynamic and thermal parameters. Product of three brackets very well explains the cross effects between the strain, strain rate and temperature on the stress flow.

$$\sigma_y = \left[A + B\tilde{\varepsilon}_p^n\right]\left[1 + Cln\left(\frac{\tilde{\dot{\varepsilon}}_p}{\dot{\varepsilon}_0}\right)\right]\left[1 - \left(\frac{T - T_r}{T_m - T_r}\right)^m\right] \rightarrow \quad (3)$$

Where A is the initial yield stress, B the strain hardening coefficient and n the strain hardening exponent. $\tilde{\dot{\varepsilon}}_p$ is the plastic strain rate, $\dot{\varepsilon}_0$ the reference strain rate, C is the strain rate coefficient, T_r and T_m are room and melting temperature respectively. m gives the thermal

softening exponent. Here the strain rate and temperature effects on the flow stress are uncoupled. This implies that strain rate sensitivity is independent of temperature, a feature that is not generally observed for most metals. The advantage of these models, however is that they are relatively easy to calibrate with a minimum experimental data in the form of a few stress- strain curves at several rates and several temperatures [1].

3.6.1 Modeling Parameters

We will briefly explain the techniques used to find the above modeling parameters [28]. Main idea is to isolate each parameter by gathering data in specific conditions and by manipulating it in the right graphics. Three curves of the equivalent flow stress versus the equivalent plastic strain must be built: one on quasi-static and isothermal conditions, two at strain related to siumulated phenomenon. Parameter A corresponds to the yield stress of the quasi-static curve. Some manipulations are required to obtain the parameters B and n.

a. Data corresponding to the elastic behavior $(\varepsilon < \varepsilon_{yield})$ is overlooked to keep only the plastic part of the curve.
b. Then Plastic data, $\sigma - \sigma_{yield}$ versus $\varepsilon_{plastic}$, is drawn in a log-log graph. Parameter B is the value $\sigma - \sigma_{yield}$ at $\varepsilon_{plastic} = 1$ and n is the slope of the curve drawn in the log-log graph.

Strain Rate parameter C is determined from the three curves at room temperature, T_{room}. A curve of the flow stress versus the logarithm of the strain rate is drawn from the datum point of each flow stress-strain curve. These datum pints represent the flow stress at different strain rates but at the same plastic strain and room temperature. Parameter C is the slope of this curve. Thermal softening exponent can be calculated by

$$m = \frac{\log(1 - \sigma/\sigma_{room})}{\log T^*} \quad where\ T^* = \frac{T - T_r}{T_m - T_r} \rightarrow \quad (4)$$

Where σ_{room} is the stress for a determined plastic strain and strain rate at room temperature, σ is the stress for the same plastic strain at high temperature

3.7 JOHNSON HOLMQUIST STRENGTH MODEL

Modern ceramic armors exhibit great resistance to ballistic penetration. Nowadays, Ceramic armoring is being promoted due to its inherent capability “Interface defeat”. Several computational ceramic models have been proposed lately, including a tensile failure model called Wilkin’s ceramic model and a micro-mechanics based model known as Rajendran-Grove model. Although it is generally agreed that ceramics exhibit high compressive and pressure dependent strength after failure, but the magnitude of this strength is in question.

Johnson & Holmquist recognized this problem and introduced a pressure dependent damage, strength and fracture model. Different variants of the said model have been proposed namely JH-1, JH-2 and JHB. Main idea was to include intact strength, failed strength, a damage model for transition from intact to failed strength and a pressure model to include bulking. The transition from intact to failed material is dependent on inelastic strain, which is also a function of pressure. JH-1 model does not soften the intact material during the damage process, but allows it to drop suddenly to the failed strength when the damage is complete ($D = 1$). JH-2 model softens the material gradually as the damage is accumulated($0 < D < 1$). The JHB model treats the damage and failed material in a manner similar to that used in JH-1 with the differences being that the JHB model uses an analytic form for the strengths of intact and failed material, and it allows for a phase change [30]. Both JH-1 and JH-2 have been implemented in AutoDyn. JH-1 has been used to accurately simulate a range of test data and does not allow gradual softening that can introduce numerical inaccuracies.

3.7.1 Strength Model

As evident from graph below, the strength is assumed to increase linearly from $\sigma = 0$ at a tensile strength of $-T$ to strength of $\sigma = S_1$ at a pressure of P_1 where T is the maximum hydrostatic tension the material can withstand. Material behaves elastically under tensile pressure until brittle failure. Once fractured, the material loses its capability to withstand any tensile loading. However the damaged material still shows considerable compressive strength as shown by the curve $D = 1$. Constants used in JH-1 model are obtained from Hopkinson bar tests.

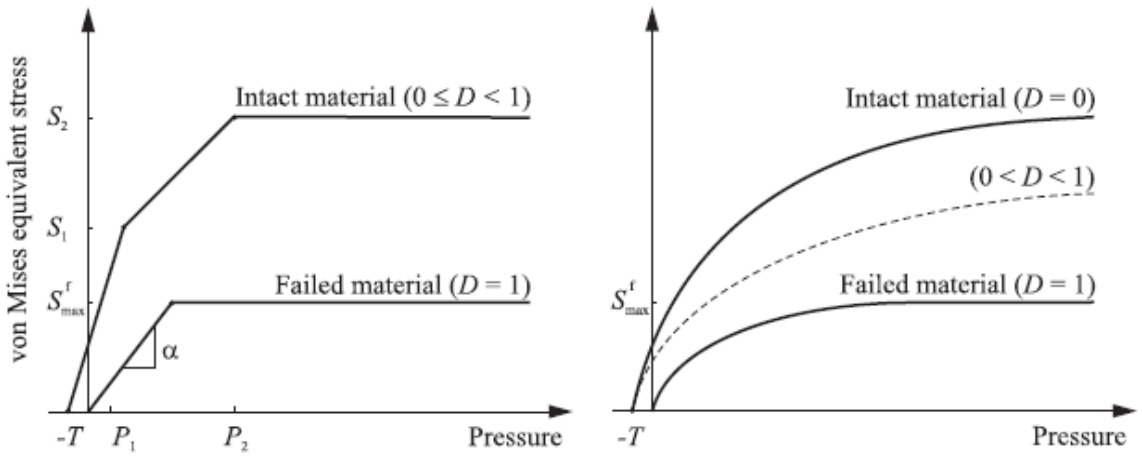

Figure 5 – Von-Mises Equivalent Stress versus Pressure in JH-1(Left) and JH-2 (Right)

3.7.2 Damage Model

Accumulation of damage to provide gradual softening with increasing plastic strain is modeled via the equivalent plastic strain $\Delta\bar{\varepsilon}^p$ and the equivalent plastic strain to failure $\bar{\varepsilon}_f^p$ at constant pressure by:

$$d = \frac{\sum \Delta\bar{\varepsilon}^p}{\bar{\varepsilon}_f^p} \rightarrow (5)$$

Where $\bar{\varepsilon}_f^p$ is given by:

$$\bar{\varepsilon}_f^p = D_1(P^* + T^*)^{D_2} \rightarrow (6)$$

With the constant parameters D_1 and D_2 as well as a pressure P^* and a minimum tensile hydrostatic pressure T^* to failure, both normalized to Hugoniot elastic limit σ_{HEl}.

3.8 SHOCK WAVE FORMATION AND EQUATION OF STATE

Unlike fluids where fluid particles travel alongside the disturbance, waves in solids are basically perturbations in the velocity field propagating through the continuum in different forms and velocities. Formation of shock wave during ballistic impact is inevitable. Such scenarios satisfy all the conditions of shock wave formation including short rise times, high pressure, density and varying temperature amplitudes. Shock waves can form as a result of both wave superposition and dispersion effects. In case of nonlinear pressure density relations, the corresponding dispersion effects lead to the formation of shock waves if faster wave components overtake earlier induced waves of lower propagation speed [29]. So, nonlinear compressive behaviour as shown below is responsible for shock wave formation in solids.

$$c^2 = \left.\frac{\partial p}{\partial \rho}\right|_s = \left.\frac{\partial p}{\partial \rho}\right|_e + \frac{p}{\rho^2}\left.\frac{\partial p}{\partial e}\right|_\rho \rightarrow (7)$$

The behaviour of material under general three-dimensional stress states is normally modelled by decomposing the stress tensor into hydrostatic (Pressure Term) and deviatoric components (Plasticity Term).

$$\sigma_{ij} = S_{ij} + \frac{1}{3}(\sigma_{11} + \sigma_{22} + \sigma_{33})\delta_{ij} = S_{ij} - p\delta_{ij} \rightarrow (8)$$

Where the spherical tensor $-p\delta_{ij}$ represents the hydrostatic pressure. Hydrodynamic material models such as the Johnson-Cook require an equation of state when used with solid elements, since hydrodynamic models only compute the deviatoric stresses. EOS is also required for the Johnson-Cook damage model when using the tensile failure criterion of dynamic spall or

pressure cut-off. For high pressures, attempts have been made to incorporate pressure dependence into the yield criterion. The hydrostatic behaviour is generally assumed to be strain rate independent. The mathematical formulation describing the behaviour among the hydro-static components of stress and strain is referred to as the equation of state of the material. Since high rate deformation involves the generation of high temperatures under shock wave conditions, temperature or energy must be considered in the formulation. EOS is the three dimensional constitutive equation which expresses the state that the material can achieve.

3.8.1 Rankine Hugoniot Relations

Change in the state variables after the passage of shock needs to be quantified. For this, conservation equations in their integral form are used to balance the conditions across both sides of the shock, with the assumption that the shock wave profile is steady in time. Following relations obtained, using the principles of conservation of mass, momentum and energy respectively, are generally known as Rankine Hugoniot equations.

$$\rho_o v_s = \rho_1 (v_1 - v_s) \rightarrow (9)$$

$$p_1 - p_o = \rho_o v_s v_1 \rightarrow (10)$$

$$p_1 v_1 = (\varepsilon_1 - \varepsilon_o)\rho_o v_s + \frac{1}{2}\rho_o v_s v_1^2 \rightarrow (11)$$

These equations relate the pressure, internal energy and density behind the shockwave to these same quantities in front of the shockwave in terms of shock velocity and particle velocity due to shockwave. Hugoniot curve is a material property which is the locus of attainable shock states and is analogous to a stress-strain curve in uniaxial stress. Although, often referred to as the EOS, Hugoniot is not a general formulation of all states but is one of the primary pieces used in the development of the EOS. While, EOS not only expresses the states that a material can achieve but also caters for the change of phase in cases where shock energy has been sufficient to melt the material.

3.8.2 Gruneisen EOS

In our case, shock energy will not be enough to set off a phase change. Hence, Mie-Gruneisen EOS has been selected to model shockwave phenomenon in metallic sheets. Mie-Gruneisen can be understood as isochoric extrapolation off the shock Hugoniot formulated as a Taylor series developed around the Hugoniot pressure.

$$p(V, e) = p_H - \frac{\Gamma}{V}(e - e_H) \rightarrow (12)$$

Where Γ is the Gruneisen constant with p_H and e_H representing the Hugoniot state.

3.8.3 Polynomial EOS

Conventionally, it was believed that ceramic fracture takes place due to tensile waves during a ballistic impact. On the contrary, it has been found that ceramic fracture is a result of high pressure induced plastic deformation, which adsorbs energy as compared to energy absorption for brittle fracture [31]. In plain words, Hugoniot Elastic limit can be understood as either the onset of fracture or the beginning of plastic deformation. As for ceramic, going from a Hugoniot which involves longitudinal stress, to an equation of state which involves pressure may not be straightforward since it requires a model for the strength of the material. Material disintegration for ceramic can be treated either as being equivalent to a phase transformation or the one involving accumulation of damage. This requires a mechanical model to account for the change in the material behaviour subsequent to the initial shock. HEL (Hugoniot Elastic Limit) values for ceramics have been observed to be quite high as compared to metals. HEL value for SiC is around 8 GPa. Polynomial EOS with bulking turned off was used for modelling shockwave phenomenon in ceramics. Here the pressure is given by:

$$p(\zeta) = k_1\zeta + k_2\zeta^2 + k_3\zeta^3 + \Delta p \rightarrow (13)$$

Where k_1, k_2 and k_3 are material constants, $\zeta = \rho/\rho_o - 1$ is the compression and Δp is the pressure increase due to dilatation and is calculated by an energy conservation argument. Δp is zero until $D = 1$ and then remains constant.

3.9 FAILURE MODEL

Damage of a material is often identified as the onset of crack formation as a result of the growth of microvoids and microcracks resulting in the degradation of material strength. It is usually characterized by a dimensionless damage variable "*D*", which is defined by the density of microcracks and microvoids δS_D lying on a plane cutting the reference volume element of cross section δS.

$$D = \frac{\delta S_D}{\delta S} \rightarrow (14)$$

Research conducted by Hancock and Mackenzie implied that void coalescence has no preferred direction and is not strictly a material constant, thereby concluding that the critical equivalent fracture strain $\tilde{\varepsilon}^f$ is a function of stress triaxiality $\tilde{\sigma}$. They modeled $\tilde{\varepsilon}^f$ as decreasing with increasing hydrostatic tension σ_H. Johnson-Cook extended the model proposed by Hancock and Mackenzie to include two more parameters. Numerically speaking,

JC is an instantaneous failure model which practically reduces the stiffness of an element to zero after erosion. Damage to an element is defined as

$$D = \sum \frac{\Delta\varepsilon}{\varepsilon_f} \rightarrow (15)$$

Where $\Delta\epsilon$ is the increment of the equivalent plastic strain occurring during an integration cycle. Fracture in materials occurs by element erosion, when D is unity. Johnson-Cook uses a linear summation concept to account for changes during the loading history. It recognizes both the changes in the failure strain with stress state, strain rate and temperature as well as the accumulation of some type of damage during the loading process [1]. General expression for strain at fracture is given by

$$\varepsilon_f = [D_1 + D_2 exp D_3 \tilde{\sigma}]\left[1 + D_4 ln\tilde{\dot{\varepsilon}}\right]\lceil 1 + D_5 T^* \rceil \rightarrow (16)$$

Where dimensionless strain rate $\tilde{\dot{\varepsilon}} = \dot{\varepsilon}/\dot{\varepsilon_o}$ with $\dot{\varepsilon_o}$ being the unity strain rate, $\tilde{\sigma} = \sigma_H/\sigma_{eq}$ while σ_{eq} is the von Mises equivalent stress given by $\sigma_{eq} = \sqrt{\frac{2}{3}\sigma_{ij}^D \sigma_{ij}^D}$. Here $D_1 - D_5$ are the fracture model parameters. We would briefly review the techniques used to obtain these parameters step by step.

3.9.1 Triaxial Stress State ($D_1, D_2, \& D_3$)

At least three axi-symmetric tensile tests are required to form the exponential curve of strain to fracture versus stress triaxiality$\tilde{\sigma}$. These tests are conducted under isothermal and quasi static conditions. Specimens in different forms are tested, each one of them having a same minimum cross section diameter. First specimen is unnotched while the second and third one's have a specifically defined notch radius. The triaxial stress data obtained for each specimen is then manipulated using curve fitting technique to graph strain to failure versus triaxial ratio. After this, the parameters giving the best curve fit are identified using least square regression.

3.9.2 High Strain Rate Stress State (D_4)

Torsion tests at different shear strain rates are performed to obtain the above parameter. These tests should cover the entire high strain rate regime being explored in the simulated phenomenon. A curve showing the strain at fracture versus the strain rate (starting from quasi-static to high strain rates) is drawn using the equivalent strain rate at fracture data obtained from these quasi-static tests. A curve of a "reduced" strain to failure $\{\varepsilon_f - (D_1 + D_2)/(D_1 + D_2)$ is drawn in the natural semi-log graph. D_4 is the slope of the curve obtained.

3.9.3 High Temperature Environment (D_5)

Same technique as D_4 can be employed to compute D_5 at high strain rate. Only this time, the shear strain to failure versus the shear strain rate is plotted at different temperatures. D_5 can then be computed by plotting the "reduced" strain to failure $\left[\{\varepsilon_f - (D_1 + D_2)\left(1 + D_4 ln\tilde{\dot{\varepsilon}}\right)\}/(D_1 + D_2)\left(1 + D_4 ln\tilde{\dot{\varepsilon}}\right)\right]$ against temperature.

Johnson-Cook model has been implemented for large strains in Autodyn using a fully vectorized backward-Euler integration algorithm for 3D, shell and 2D analysis. The crack growth is simulated by an element killing procedure which removes the element when the damage reaches its critical value D_c. Johnson [33] also suggested a non-dimensional parameter $\rho V^2/Y_d$ to categorize the impact between two metallic bodies. Physically, ρV^2 is the stagnation pressure of the projectile seen as fluid jet. While Y_d is the target strength. As the ratio $\rho V^2/Y_d$ exceeds 1, the inertia of the impacting projectile becomes dominant over the target yield strength.

CHAPTER-4

4. ANALYTICAL MODELING

Analytical techniques for solving ballistic impact problems capture a fair share of solution space. These models are based on algebraic relations and ordinary differential equations which do not need large computational resources [20]. They may vary from simplified one dimensional equation covering a single physical phenomenon to two/three dimensional models based on local and global interactions and respective deformation with different failure criterion. Each model is derived considering a common goal of predicting Ballistic Limit Velocity and Residual Projectile velocity for a specific shield. Analytical models are usually based on qualitative laws which can be further used to develop new theoretical models and carry out further experimental work [20]. These models might not be sufficiently reliable depending on the approach being used for their derivation and the model giving accurate predictions in one case might not bear the same result in another scenario. Ben-Dor et al. published a review covering models classified as empirical, semi- or quasi-empirical, engineering, simplified, analytical, semi-analytical and approximate dealing with the mechanics of high-speed ballistic penetrations.

4.1 LOCALIZED INTERACTION APPROACH

This is the most commonly used approach in the domain of analytical modeling. Herein the integral effect of the integration between host medium and a moving projectile is described as a superposition of the independent local interactions of the projectile's surface elements with the medium [23]. Each local interaction is determined both by the local geometric and kinematic parameters of the surface element (primarily, by the angle between the velocity vector and the local normal vector to the projectile surface) and by some global parameters that take into account the integral characteristics of the medium e.g., hardness, density, etc. It is very attractive to apply the localized interaction approach for investigating problems of impact dynamics, since it allows one to describe relatively easily the projectile-medium interaction—taking into account the projectile shape—and to simulate the motion of a projectile in a shield. It is the most widely used analytical modelling approach and most of the work published by Ben-Dor is based upon LIM.

4.2 CAVITY EXPANSION APPROXIMATION

Second one is the Cavity Expansion Approximations, in which expansion of a spherically symmetrical cavity from a zero initial radius at a constant velocity is considered by means of some continuum mechanics model of the material. The study of Bishop et al. pioneered the application of cavity expansion models in penetration mechanics. They obtained solutions

describing the quasi-static expansion of cylindrical and spherical cavities in an infinite medium from zero initial radius and used these solutions to determine the forces acting at a conical projectile [23]. Solution of cavity expansion approximation models is usually given by

$$p = \widetilde{w}(\vec{a}; y) \quad \rightarrow (17)$$

Where p is the stress at boundary of the cavity, y is the radius of the hole. The normal stress at the surface of the projectile moving in the same direction is given by

$$\sigma_n = \widetilde{w}(\vec{a}; uv) \quad \rightarrow (18)$$

Which means the normal stress caused by the target-projectile interaction at the projectie's surface at some location moving with the instantaneous normal velocity $v_n = v\cos\hat{v} = uv$ is equal to the stress at the boundary of the cavity that expands with constant velocity v_n. SCEA (Spherical Cavity Expansion Approximation) and CCEA (Cylindrical Cavity Expansion Approximation) are the two most commonly used variants of this technique.

In CCEA, studying the normal penetration of a slender body, it is assumed that the target material moves in the radial direction. Dividing the target into infinitely thin layers, each layer is studied on account of the cavity expansion caused by the impacting projectile. This approach gives the stress at the boundary of hole in each layer and subsequently the force acting on the projectile at each location on the projectile's lateral surface.

4.3 LAMBERT-JONAS APPROXIMATION

After studying various empirical and semi-empirical models, Lambert and Jonas presented a unified relation for assessing Ballistic Impact They proposed a power law relation between impact, residual and ballistic limit velocity. Many of the empirical and semi-empirical models can be represented in the form of Eq-1, particularly, models based on energy and/or momentum conservation. Mileiko and Sarkisyan and Mileiko et al. demonstrated that a solution of the equation of motion of the projectile yields Eq-1 with $a_0 = 1$, when power-law dependence between the projectile's drag force and its velocity is valid. Nixdorff showed that under certain assumptions the theory of Awerbuch and Awerbuch and Bodner implies Eq-1. Ben-Dor et al. compared the accuracy of Eq-1 with an arbitrary exponent n and that with $n = 2$. Garbarek and Andreson et al. considered Eq-1 as only one of the possible correlations between $\hat{v}_{res}$ and $\hat{v}_{imp}^{n}$, and used a different unified relationship.

$$\hat{v}_{res} = (a_2 z^2 + a_1 z + a_0 z^{0.5})/(z+1)\,, z = \hat{v}_{imp} - 1, z \leq 2.5 \;\Rightarrow\; (19)$$

Where the approximation coefficients $a_i (i = 0,1,2)$ are determined from regression analysis of experimental data.

Bodner states, “The point could be raised whether developing more complicated models of ballistic perforation is worthwhile since it may appear to bring the procedure closer to that of the full numerical solution.”

4.4 COMMONLY USED ANALYTICAL MODELS AND THEIR APPLICATION

Many analytical models have been proposed to assess the ballistic performance including Wen and Jone, Bodner, and Bai and Johnson. Then Recht and Ipson presented a discrete version of localized interaction theory using ballistic pendulum technique and assuming shear plug formation to be the only failure mechanism. Their model was limited due to the requirement of prior knowledge of BLV and single failure mechanism. Dynamic cavity expansion models are considered to be the most effective analytical tools available to study the dynamics of a rigid projectile. Using this technique, a major breakthrough was achieved by Chen and Li [32]. They presented a penetration model for thick plates with projectiles of various nose shapes. The model incorporated two perforation mechanisms: hole expansion and plug formation for sharp and blunt nosed projectiles respectively. In addition to the localized shear deformation at the peripheral of the central plug, their rigid plastic structural model also considered the effect of plate bending and membrane stretching. The local indentation/penetration employs a dynamic cavity model [32]. They have recently updated their model to cover the failure modes ranging from shear plugging to adiabatic shear plugging with the increasing target thickness. They formulated the Ballistic limit of target and residual projectile velocity as

$$V_{BL} = 2\sqrt{\frac{2\chi(1+\eta)(\eta+\vartheta)}{\sqrt{3}}}.\sqrt{\frac{\sigma_y}{\rho}} \quad \rightarrow (20)$$

$$V_r = \frac{\vartheta V_i + \eta\sqrt{(V_i^2 - V_{BL}^2)}}{(1+\eta)(\eta+\vartheta)} \quad \rightarrow (21)$$

Where $\chi = H/d$ with H being the thickness of circular target plate and d the diameter of impacting projectile. Also $\eta = \rho\pi d^2 H/4M$ with M being the mass of projectile. Whereσ_y & ρ are the yield stress and density of target material.

Two component composite armour is one of the most widely used configurations, with ceramic sheet as the front plate and a ductile back plate usually Aluminium. Hard plate in front usually erodes and decelerates the impacting projectile while the ductile back plate captures the remnants of eroded projectile. Florence developed an analytical model to

accurately predict the ballistic performance of such target configurations impacted normally by a rigid projectile. This model was later re-worked by Hetherington and Rajagopalan.

$$v_{bl}^2 = \frac{\varepsilon_2 \sigma_2 b_2 z[(\gamma_1 b_1 + \gamma_2 b_2)z + m]}{0.91m^2}, \quad z = \pi(R + 2b_1)^2 \quad \rightarrow (22)$$

Where b_i are the plate's thickness, σ_i the ultimate tensile strength, ε_2 is the braking strain, γ_i are the densities of the target materials, and subscripts 1 and 2 refer to the ceramic and back plate respectively. Florence's model has been found to be the most suitable technique for solving problems related to armour optimization.

Ben-Dor et al. [1998b; 1998a; 1999b; 1999a; 2000; 2006a] studied analytically the influence of air gaps between the plates and the order of plates on the BLV of a multilayered shield against conical shaped impactors, and the results are summarized in [Ben-Dor. et al. 2006a]. They found that, for the wide class of impactor-shield interaction models, the ballistic performance of the shield is independent of the widths of the air gaps and of the sequence of plates in the shield and that it is determined only by the total thickness of the plates if the plates are manufactured from the same material. Using the two-term impactor-shield interaction model, they found the criterion (depending on mechanical properties of the materials of the plates) determining the order of plates in a multilayer shield that provides the maximum BLV. This criterion remains valid for the projectiles with a shape different from conical.

CHAPTER-5

5. NUMERICAL SETUP

During this chapter, we would define the required parameters and inputs for FEM simulations of projectile impact on monolithic as well as multi-layered sheets. For monolithic sheets, a circular plate of Diameter 500 mm and thickness 10-20 mm were chosen as targets. For multi-layered sheets, target was made up of two or three sheets bonded together of either similar or varying thickness. A blunt cylinder of diameter 20 mm and 80 mm length was selected as the projectile. Initially, material of projectile was selected to be Arne Tool Steel as used by Borvik in its experimental study of the ballistic impact of blunt projectile on Weldox 460E steel plates of varying thickness.

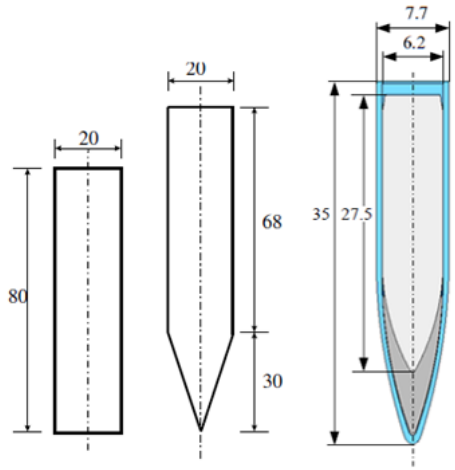

Figure 6 – Dimension of Three Projectiles: Blunt, Conical and 7.62 mm Bullet

Steel 1006 with Johnson-Cook material model was also used as projectile to capture the deformation in projectile during impact. All simulations were carried out with the projectile moving at a velocity of 200-500 m/s, mainly to identify a single performance parameter for different armor options. Initially both the projectile and target were modeled as 3D geometries to study if the selected scheme addressed all penetration problems. Critical impact area was assumed to be five times the projectile diameter; this was kept in accordance with the range of 3-6 times proposed by Zukas. This assumption was applied to constitute a coarser mesh towards the outer boundary of the plate. Also, symmetry conditions were used to reduce the number of elements by 75% and hence the computational time.

There is another issue which should be addressed before going for final simulation that is the hourglass energy. Despite being a robust solution for large deformations and high strain rates and at the same time saving extensive computational time, the one-point (reduced) integration technique used in ANSYS Explicit Analysis is prone to zero-energy modes. These modes,

commonly referred to as hourglassing modes, are oscillatory in nature and tend to have periods that are much shorter than those of the overall structural response (i.e., they result in mathematical states that are not physically possible) [35]. They typically have no stiffness and give a zigzag appearance to a mesh known as hourglass deformations [35]. In other words, the hourglass mode does not result in any kind of strain and therefore has no contribution in the energy integral. Although this problem cannot be eradicated altogether while using brick and quadrilateral shell or 2D elements. A straightforward solution to hourglassing is to use a uniform & refined mesh during numerical simulations. A simple check proposed by ANSYS is that the hourglassing energy should always be less than 10% of the internal energy.

For 3D simulations, element size in the critical impact region was kept to 0.001 m. For 2D simulations, element size of 0.0005 m was used for both the target and projectile, as much fine mesh can be chosen keeping in view the relief in computational time as compared to 3D simulations.

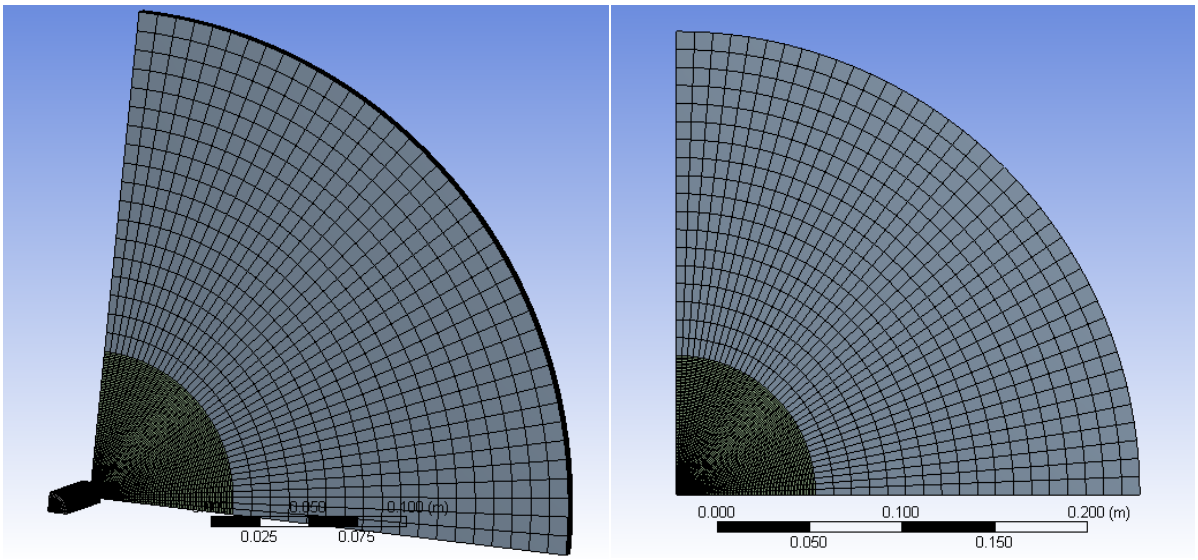

Figure 7 – Mesh in case of Blunt Projectile

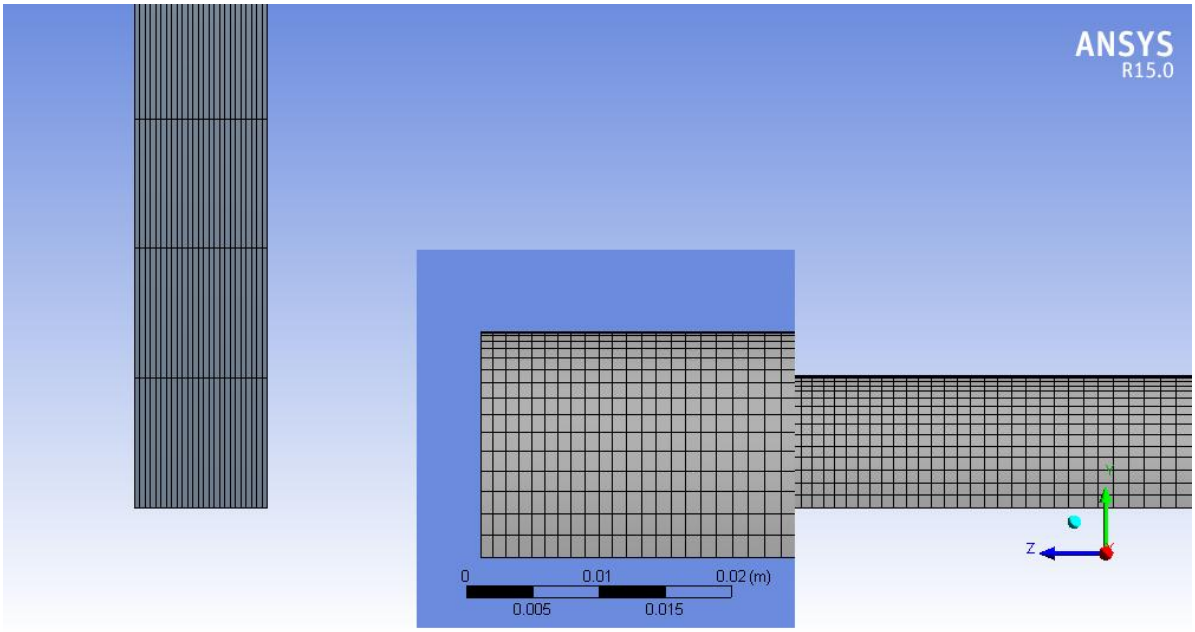

Figure 8 – Mesh Closeup

As evident from above figure, a biasing factor is used to adjust the spacing ratio of nodes on the projectile. This feature comes in handy as the left edge withstands severe deformation as compared to the far edge of the projectile. Rightly so, the nodes are clustered towards the impacting edge of projectile using a biasing factor of 3.

AutoDyn gave two options: one to use ideal scenario and model all the projectile-target interaction as frictionless and two to include a friction coefficient. While modeling the penetration of blunt projectile inside a target sheet, frictional effect was ignored primarily due to the absence of thin film between the two interacting surfaces [37]. This is primarily because, as the blunt projectile hits the target, its front edge deforms resulting in a mushroomed shape. As the front end of projectile penetrated through the target, it resulted in a cavity usually bigger than the diameter of rest of the projectile body. So the remaining projectile body is hardly in contact with the target.

In case of conical and ogival projectiles, projectile penetration induced a thin film between the two interacting surfaces which called for careful selection of appropriate friction coefficient [38]. Also, the projectile with sharp nose slides along the lateral surfaces of the hole formed during penetration. Ballistic results for three different values of friction coefficients were compared both for Al and Steel targets. Values of 0.05, 0.08 and 0.1 were finalized for all steel targets based on the assumption of Ravid and Bodner [39]. While the values of 0.0, 0.02 and 0.05 were used for all Al targets [38].

In case of steel, very little variation in the residual velocity was observed for three different values of friction coefficients. Although the value of 0.1 gave accurate approximation of Ballistic Limit Velocity, subsequent increase in impact velocity didn't give much accurate results. So a relatively median value of 0.08 was selected for future simulations.

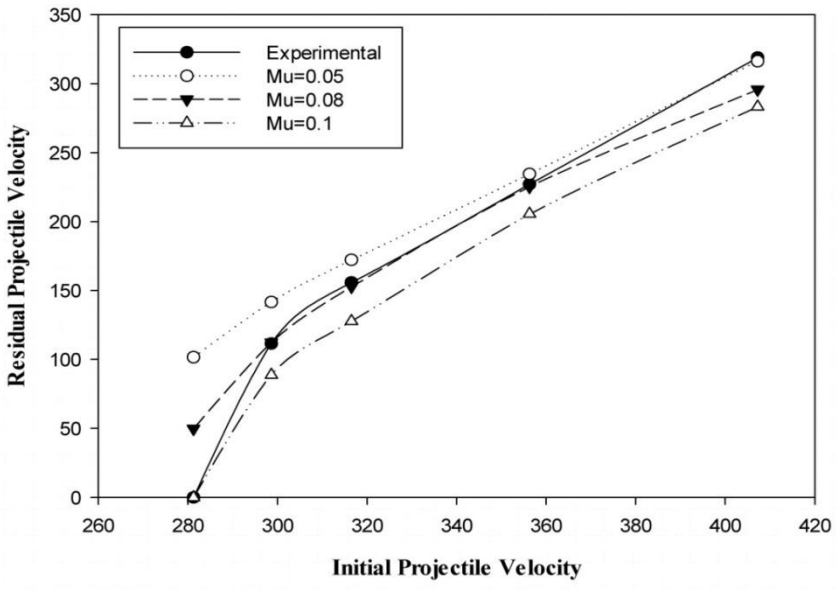

Figure 9 – Comparison of Friction Coefficients values (Steel)

Now, in case of a 15 mm thick Al5083-H116 target sheet, numerical results were more sensitive to the change in friction coefficient as compared to Steel. On average, $\mu = 0.02$ gave relatively accurate results as compared to 0.0 and 0.05 and was adopted for subsequent simulations.

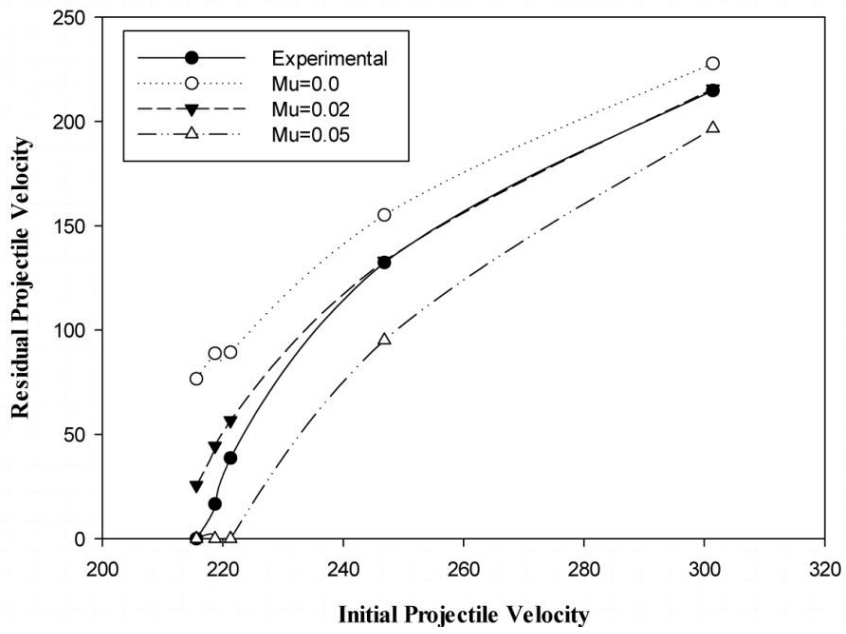

Figure 10 – Comparison of Friction Coefficients values (Al)

Brick Element (solid) eight node hexahedron in 3D and shell element in 2D were used.

Given the projectile and target shape, structured mesh seemed to be a practical and viable option. Total number of elements for blunt faced 3D projectile is around 12800 while the number of elements for a 10 mm 3D circular plate was 93000. At the same time, the number of elements for 2D ogival nosed projectile and target plate were 1592 and 50000 respectively.7.62 mm projectile was modeled as three independent sections bonded together with a brass jacket, steel core and lead filler. 2D geometry was generated using existing sketches and cross section views. While keeping the same mesh configuration for target plates in case of blunt and conical nose projectiles, it was impossible to model the same structured mesh for conical shaped projectiles. So a hybrid approach using structured as well as unstructured mesh was used in case of 7.62 mm Bullet.

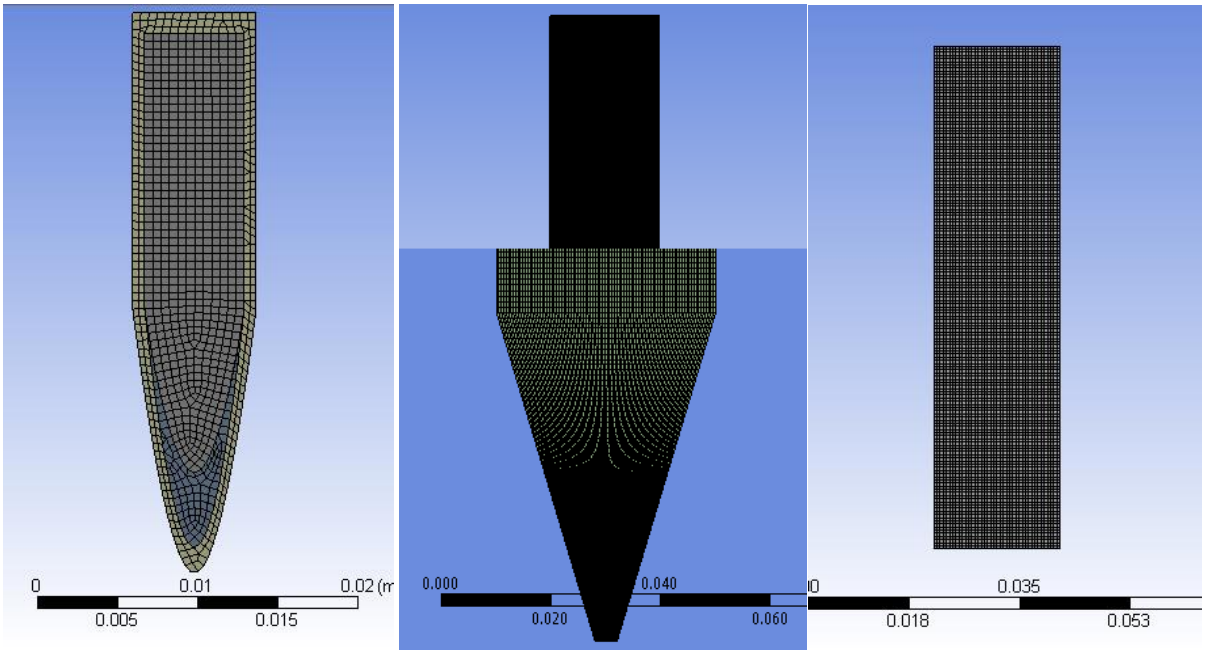

Figure 11 – Mesh Detail for each Projectile Shape

Borvik observed that the numerical results were quite sensitive to mesh sizes in case of blunt projectiles as compared to conical nose projectiles [40]. Therefore, a mesh independence study was carried out to check the effect of different mesh sizes and also the numerical accuracy of computational solution. For this, a blunt projectile was tested against a 10 mm thick Weldox 460 E target at an impact velocity of 277.5 m/s. Experimentally the residual velocity of the projectile was measured to be 197.9 m/s [3]. Mesh size was steadily increased up to $1.2 \times 1.2\ mm^2$ and the residual velocity in each case was noted and compared with the experimental result. Following table shows the variation in residual velocity and computational time for each case.

Table 1- Mesh Independence Study

Mesh Nomenclature	Minimum Element (mm^2)	Residual Velocity (m/s)	% Error	CPU Time (Hr)
M1	$0.1X0.1$	201.6	1.86	7.7
M2	$0.2x0.2$	202.2	2.17	6.2
M3	$0.25x0.25$	206.7	4.44	6.1
M4	$0.5x0.5$	211.8	7.02	3.6
M5	$1.2x1.2$	252.6	27.6	1.9

For mesh size greater than1.2×1.2, an error of 27.6 % was observed which is far greater than the threshold of 5%. Polynomial EOS with bulking turned off was used for modeling shockwave phenomenon in ceramics while shock EOS linear model was used for metallic targets.

Table 2- Material Parameters for SiC-B [34]

Density $(\boldsymbol{\rho})$ $\boldsymbol{kg/m^3}$	**HEL** GPa	Intact Strength CC GPa				Failure Strength CC		$\boldsymbol{\varepsilon^f_{max}}$	**Tensile Strength** GPa	**G** GPa	$\boldsymbol{\beta}$
		$\boldsymbol{S_1}$	$\boldsymbol{P_1}$	$\boldsymbol{S_2}$	$\boldsymbol{P_2}$	$\boldsymbol{S^f_{max}}$ $\boldsymbol{(GPa)}$	$\boldsymbol{\alpha}$				
3227	11.7	7.1	2.5	12.2	10	1.3	0.4	1.2	0.75	193	1
$\boldsymbol{k_1}$ $\boldsymbol{(GPa)}$				$\boldsymbol{k_2}$ $\boldsymbol{(GPa)}$			$\boldsymbol{k_3}$ $\boldsymbol{(GPa)}$				
220				361			0				

Johnson-Cook strength and damage model were used for ductile while JH-1 was used for brittle target materials. Standard material parameters available in ANSYS library didn't account for all the ballistic events. A comprehensive literature review was carried out to search for the material parameters required to model Johnson-Cook strength and failure models for metallic targets and JH-1 model for Silicon carbide target. Following material parameters were selected after thorough literature review.

Table 3 - Material Properties and Modeling Parameters for Metallic Shields

Sr. No	**Parameter**	**Unit**	**Al 7075 T651**	**Al5083 H116**	**Weldox 460E**	**Steel 1006**	**Steel 4340**
1	Density ρ	kg/m^3	2810	2700	7850	7850	7850
2	Specific Heat C_p	$J/kg.K$	910	910	452	486	475
3	Johnson Cook Strength						
3.1	Initial yield Stress A	MPa	520	167	490	350	792
3.2	Hardening Constant B	MPa	477	596	807	275	510
3.3	Hardening Exponent n	----	0.52	0.551	0.73	0.36	0.26
3.4	Strain Rate Constant C	----	0.0025	0.001	0.0114	0.022	0.014

3.5	Thermal Softening Exponent m	----	1.61	0.859	0.94	1	1.03
3.6	Melting Temperature	K	893	893	1800	1811	1793
3.7	Shear Modulus G	GPa	26.9	27	75	79.6	79.6
4	Shock EOS Linear						
4.1	Gruneisen Coefficient Γ	----	1.97	2.02	1.707	1.587	1.707
4.2	Parameter C_0	m/s	5240	3940	3850	3075	3850
4.3	Parameter S	----	1.4	1.498	1.354	1.294	1.354
5	Johnson-Cook Failure						
5.1	D1	----	0.096	0.178	0.0705	-0.8	0.05
5.2	D2	----	0.049	0.389	1.732	2.1	3.44
5.3	D3	----	3.465	-2.25	-0.54	0.5	2.12
5.4	D4	----	0.016	0.147	-0.015	0.0002	0.002
5.5	D5	----	1.099	16.8	0	0.61	0.61

Whenever the projectile comes in contact with the target material, nature of that interaction needs to be defined. Especially in large deformation problems like ballistics, accurate modeling of contact interfaces is required for comparable numerical results. With the contact detection set to trajectory, ANSYS AutoDyn provided two options: “Penalty contact constraint” which was based on the size of contact segment and its material properties and the “Decomposition response”, where the system response to detected contact was computed to conserve energy and momentum. As compared to the penalty method, the decomposition response algorithm was more impulsive and gave rise to high hourglass energies and energy errors [36].

During all simulations, it was assumed that the projectile impacted at exactly right angle on the target sheet. A velocity probe was placed at the rear end of projectile to keep track of the projectile velocity during penetration as the front end may be severely deformed in certain cases. Initially, a temperature probe close to impact region was placed at the surface of top plate to check if there is any drastic variation in temperature during penetration process. Another temperature probe was placed at 150 mm from the plate centre to compare the

temperature variation results. Target's circumferential peripheral was modeled as a fixed support in all cases.

CHAPTER-6

6. NUMERICAL RESULTS AND THEIR COMPARISON

In military and civilian applications, optimization of metal shields against projectile impacts has long been of interest. During the course of study, several target configurations that consist of parallel layers and monolithic plates will be investigated. Initially, numerical simulation based on the experimental data from the likes of Borvik [2, 3] will be carried out. Purpose of this activity will be twofold; it will not only be a benchmark for validating our computational results but will also play a pivotal role in determining the critical computational parameters and techniques.

6.1 BLUNT PROJECTILES AGAINST MONOLITHIC SHEET

Initially, simulations were carried out for Weldox 460E due to the vast amount of experimental and numerical data available for comparison. I started with the case of a blunt projectile of Arne Tool Steel impacting a circular plate of thickness 10, 12, 16 & 20 mm respectively. Projectile was moving at a velocity of 500 m/s.

Energy summary was recorded during the course of entire simulation. As soon as the projectile hit the target, a drop in kinetic energy was observed while the same amount of energy that is 604.8 J appeared as the internal energy precisely. Hence the condition of energy conservation was satisfied. As discussed earlier, explicit hydrocodes use reduced point integration to get rid of locking phenomenon which in turn gives rise to spurious deformation modes. So, next task was to check for the hourglass energy, as AutoDyn used hour glass control to deal with zero energy modes. Hourglass energy lied within the threshold value of 10 % of the internal energy as suggested by ANSYS. This does not necessarily stamp the authenticity of simulation results but effectively rules out a major issue.

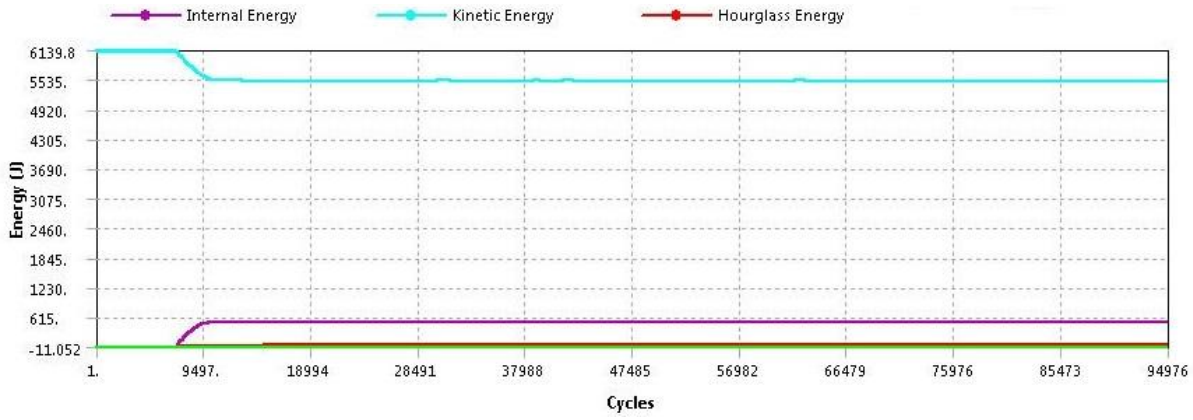

Figure 12 – Hourglass Energy

Following stress contours are for a 10 mm Weldox 460E target hit by a blunt projectile. As

soon as the projectile hits the target, a compressive wave is generated due to which the projectile and target material tends to flow away from the impact region. Emanating from the point of impact, a lateral stress wave can be observed moving away from the impact origin gradually.

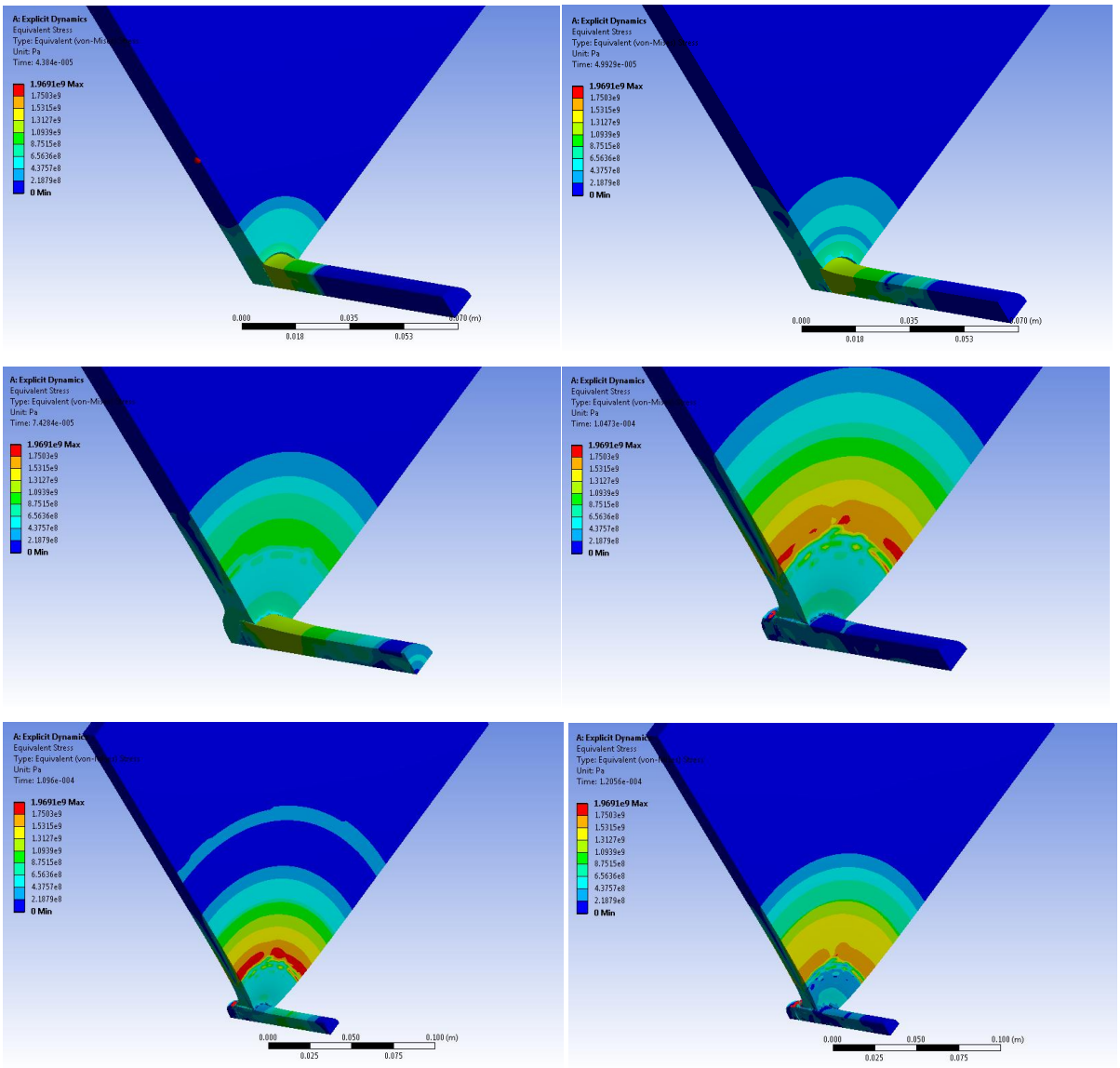

Figure 13 - Stress (Von-Mises) Contours at $t = 43.8, 49.9, 74.2, 104, 109$ & 120 μs

This shockwave is reflected back from the far end of target.

The target failed primarily as a result of plugging which is the most commonly observed scenario in case of blunt projectiles. Sharp edges of the projectile induce crack formation in their circumferential vicinity. A cylindrical plug nearly the size of projectile can be observed being ejected from the rear end of the target. This is exactly in agreement with the proposition by Woodward, which says that plugging is the dominating failure mode with the thickness of target plate being less than $\sqrt{3}d_p/2 = 17.3\,mm$, where d_p is the diameter of

projectile. Having established that, such failures are never really dominated by one mode. As evident from figure-8, a slight amount of ductile hole enlargement can also observed. Strain rate finally settles down to a value of around $4.71 \times 10^4/s$. Being a failure mode dominated by adiabatic shear, deformation is mostly localized around the sharp edges of the projectile as evident in the following figure.

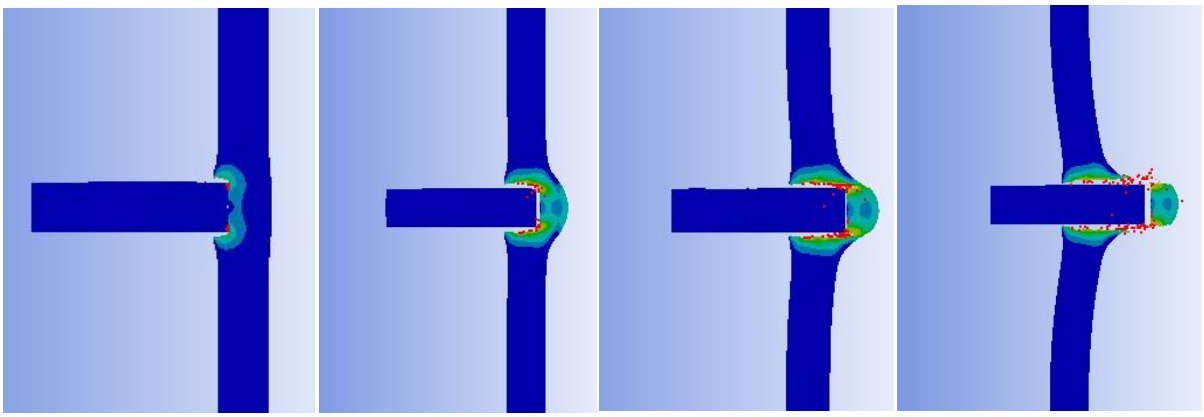

Figure 14 – Penetration at T=30, 60, 100 & 150µs in Weldox 460E

A visible gap can be observed between the projectile body and cavity perimeter. There is hardly any contact between the projectile's body and target as the projectile penetrated through the target. Following graph has been plotted for ten different input velocities starting from 131.3 m/s to 400 m/s. No curve fitting technique was used. Ballistic limit velocity for above target was found to be 166 m/s. A steep drop in residual velocity was observed below an impact velocity of 175.2 m/s.

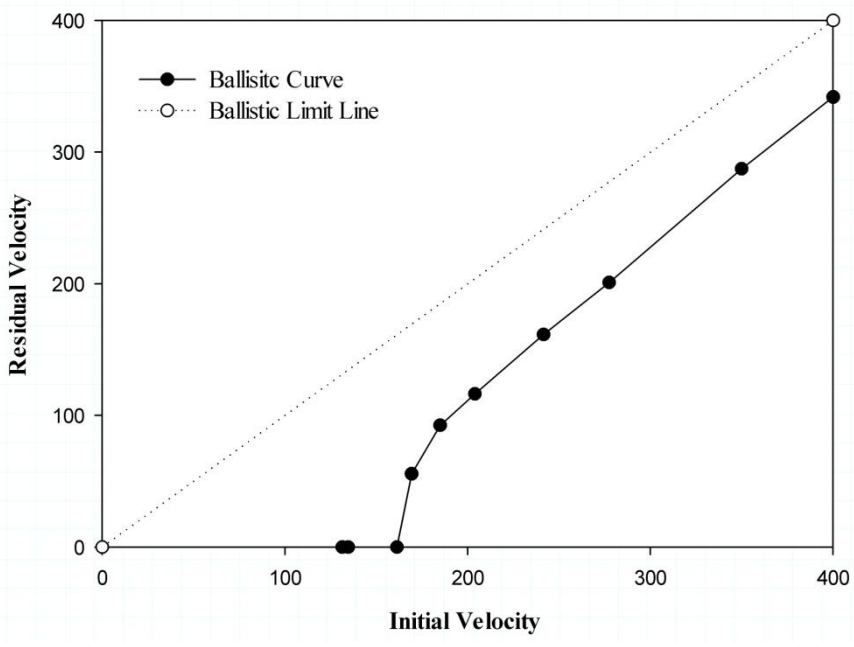

Figure 15 – Ballistic Curve for 10 mm thick Weldox 460E Target

Next step was to compare the numerical data with experimental [2,3] and analytical results.

Analytical solution was computed using the model proposed by Chen and Li based on the rigid plastic analysis of plug motion and local penetration process [41]. As evident from the graph given below, numerical results are quite comparable to the empirical data. Maximum underestimation of 6.67% was observed for numerical results while an overestimation of around 9% was observed in case of analytical solutions.

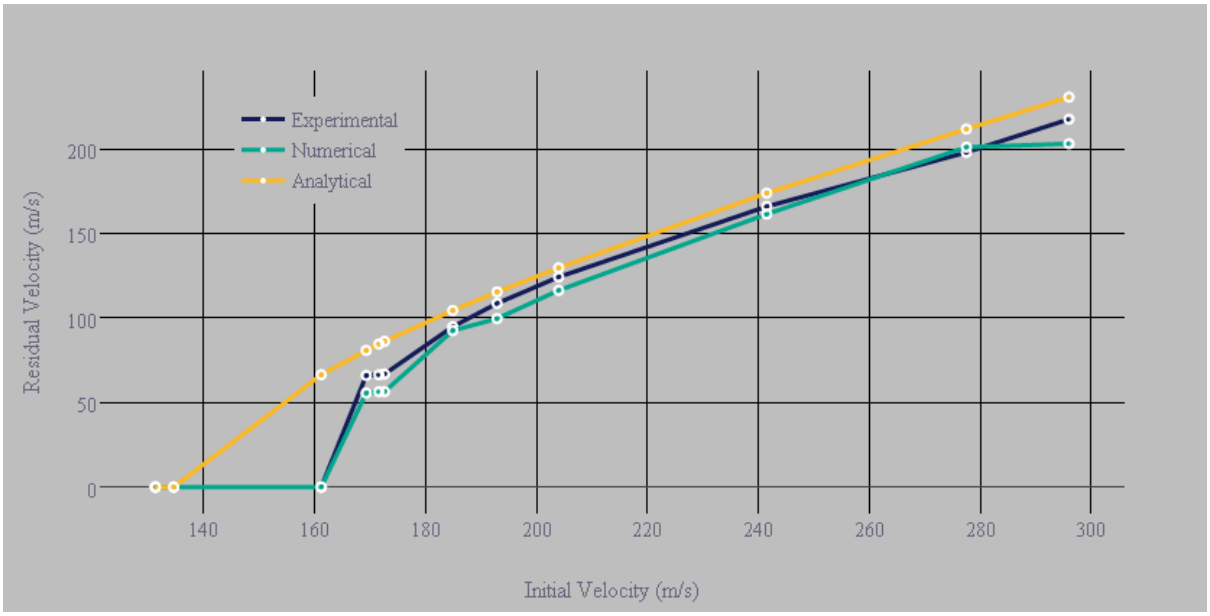

Figure 16 – Comparison of Experimental [3], Analytical & Numerical Solution Weldox 460E

Experimental results lied in between the numerical and analytical ones. While deriving the analytical model, Chen and Li assumed that the projectile and plug have the same residual velocity after perforation. So a quick comparison was carried out to check if the above mentioned assumption is accurate.

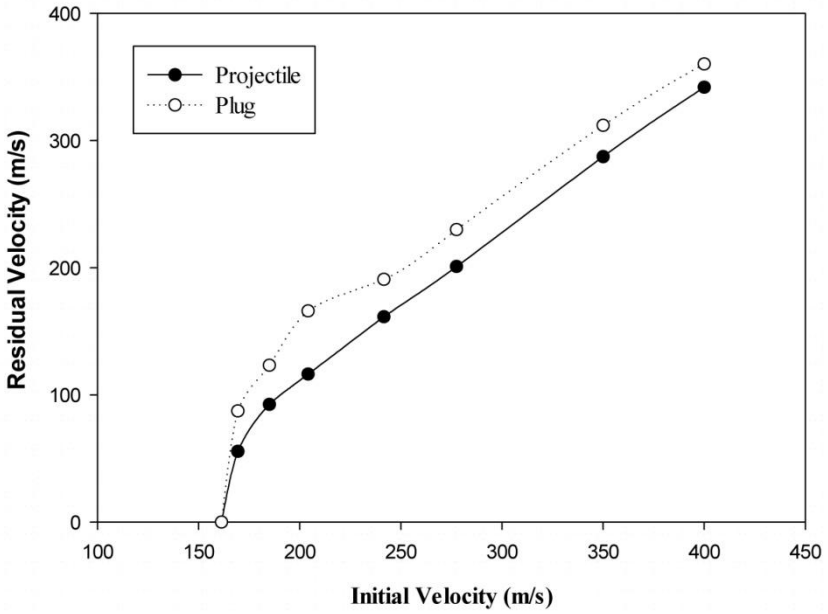

Figure 17 – Comparison of Plug and Projectile Residual Velocity

Above graph shows that there is a marked difference between the residual velocity of projectile and plug. An average difference of 30.5 m/s was observed with the plug residual velocity on the higher side. Overestimation in case of analytical results can be attributed to the fact that the model proposed by Chen and Li is based on the yield strength of the target material, which is a simplified approximation of a very complex problem.

Following graph shows the maximum deformation plotted against increasing impact velocities for a 10 mm Weldox 460E target. Regression analysis was done to fit a line through the computed data. Amount of deformation undergone by the target increases with gradual decrease in velocity. Amount of target deformation becomes really sensitive to the change in initial velocity as it dropped below 190 m/s.

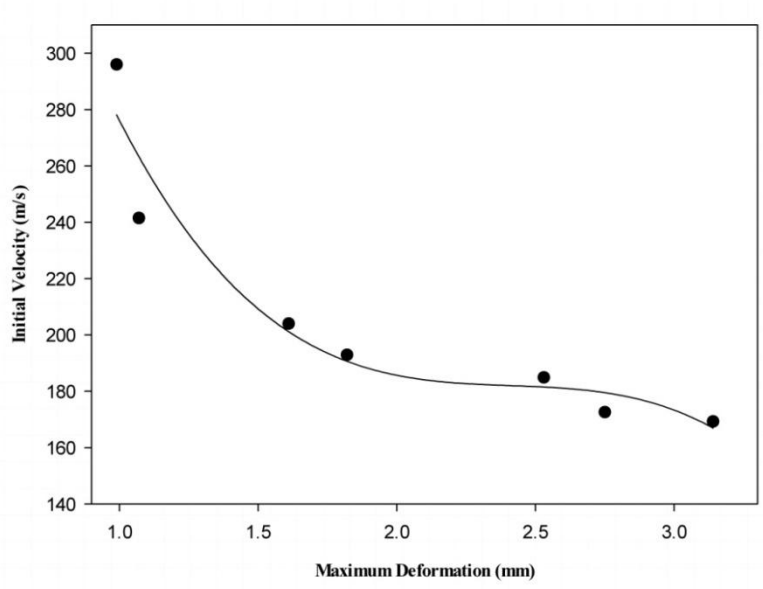

Figure 18 – Variation in Maximum Deformation with Initial velocity

Following graph has been plotted for a blunt projectile moving at a velocity of 169 m/s, impacting against a 12 mm Weldox target, to check the contact force behavior with time.

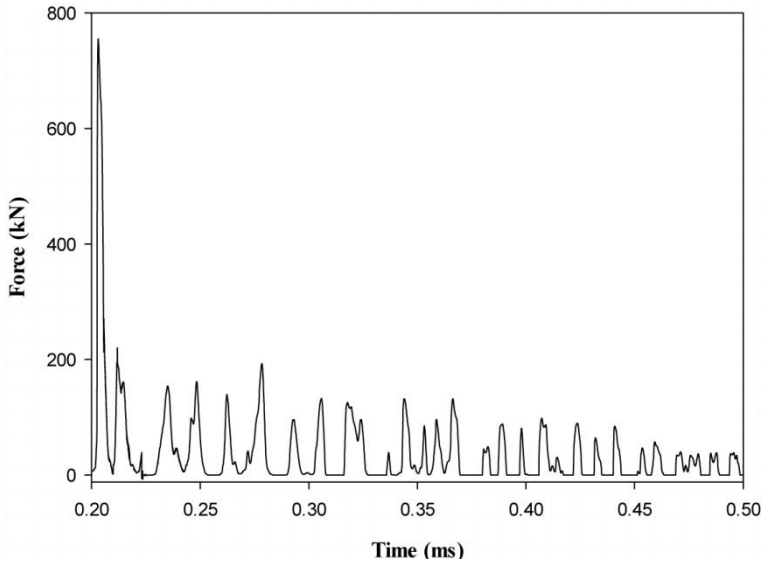

Figure 19 – Contact Force Plot

It was observed that as soon as the projectile hits the target, a sudden spike can be observed in the graph for a very small time. Subsequently a steep drop was observed after first contact followed by small magnitude oscillations. Contact force then finally settled down to zero. These oscillations can be attributed to the fact that after first contact, projectile continuously tried to penetrate through the target giving rise to short duration elastic plastic shock waves. These waves are then reflected back from the far end of target. Also there is continuous interaction between the projectile and plug until the projectile achieves complete perforation at 0.5 milliseconds approximately.

Another important factor to look for was the evolution of projectile velocity over the course of time. For an initial velocity of $500\ m/s$, there was a sheer drop in projectile velocity from $500\ m/s$ to $463.2\ m/s$ during the time interval of just 20 μs. Then for the next 80 μs, a rather slow change in velocity was observed, before finally settling down to a constant value of 446.5 m/s.

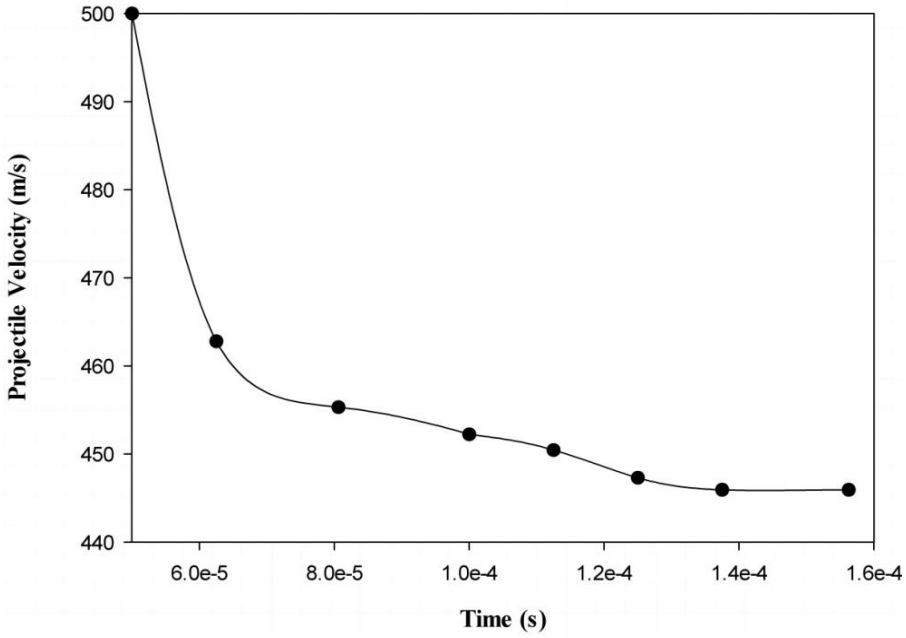

Figure 20 – Velocity Contour

Visible change in the kinetic energy of projectile can be observed before and after impact. Obviously, this reduction in kinetic energy can be attributed to the work carried out by projectile during perforation. This is a very critical phenomenon to be considered while designing a ballistic resistant shield. It depends on the amount of energy absorbed by the target. According to Borvik, transformation of this kinetic energy can be observed in three different forms: Global target deformation, Failure including Localized plastic flow and Projectile deformation. Overall work done by the projectile was calculated using the change in projectile kinetic energy. So an expression encompassing simple energy conservation was used that is

$$\Delta K.E = \frac{1}{2} m_p (v_i^2 - v_i^2) - \frac{1}{2} m_{pl} v_{rpl}^2 = W \ \rightarrow (23)$$

It is a simple expression stating that total work done is equivalent to the change in projectile's kinetic energy. Using the above methodology, following graph has been plotted for the work done by a blunt projectile impacting against a 12 mm Weldox target.

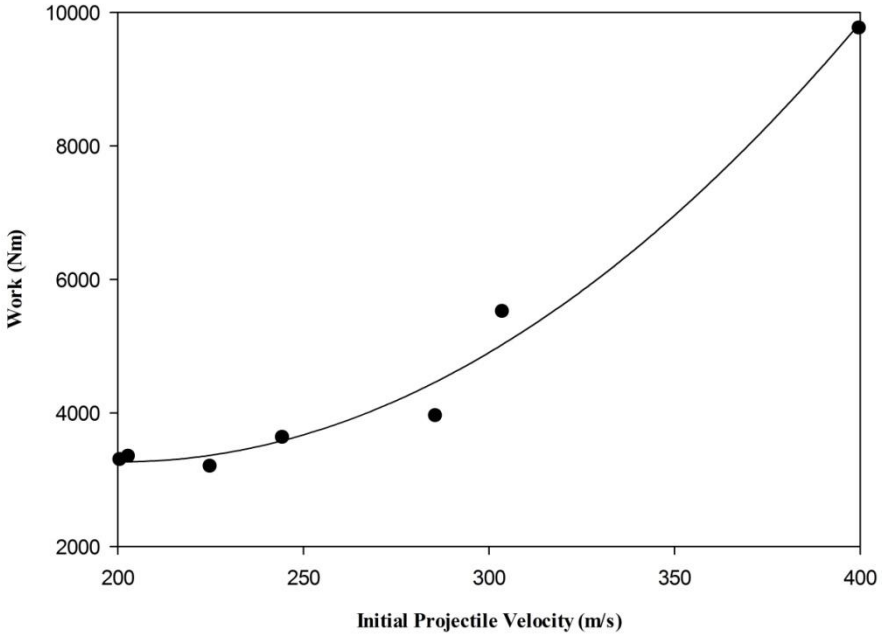

Figure 21 – Work Done

Amount of energy absorbed by the projectile increased almost linearly with the increase in initial velocity.

Following graph has been plotted for a blunt projectile impacting against a 16 mm Weldox target.

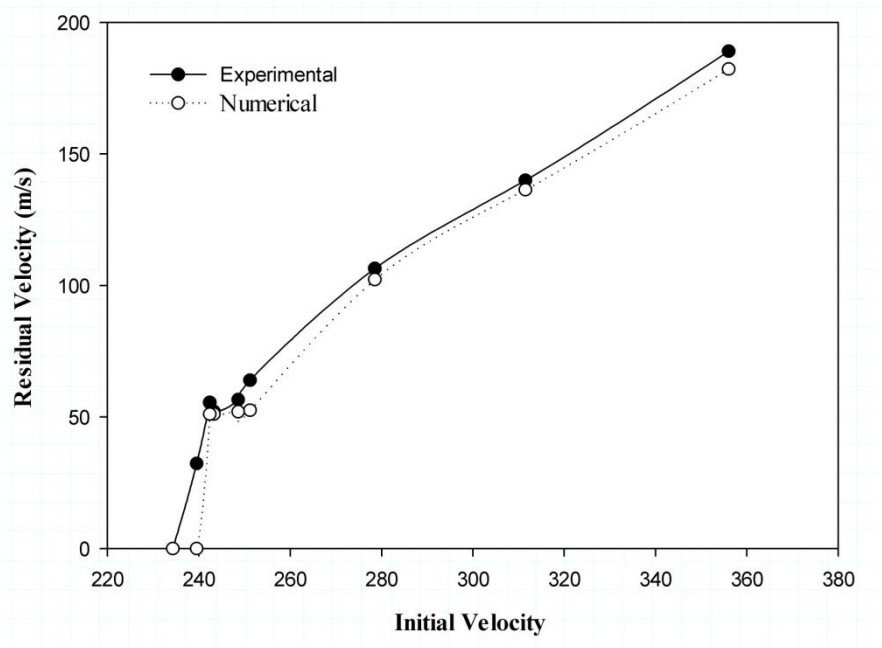

Figure 22 – Comparison of Experimental [3] & Numerical Solution Weldox 460E

Numerical results are in agreement with the experimental data with a maximum error of

Increase in the impact velocity significantly reduced the damage zone due to rapid damage localization. As the impact velocity was increased, more localized damage was observed.

Following results have been plotted for a 20 mm Weldox target against a blunt projectile.

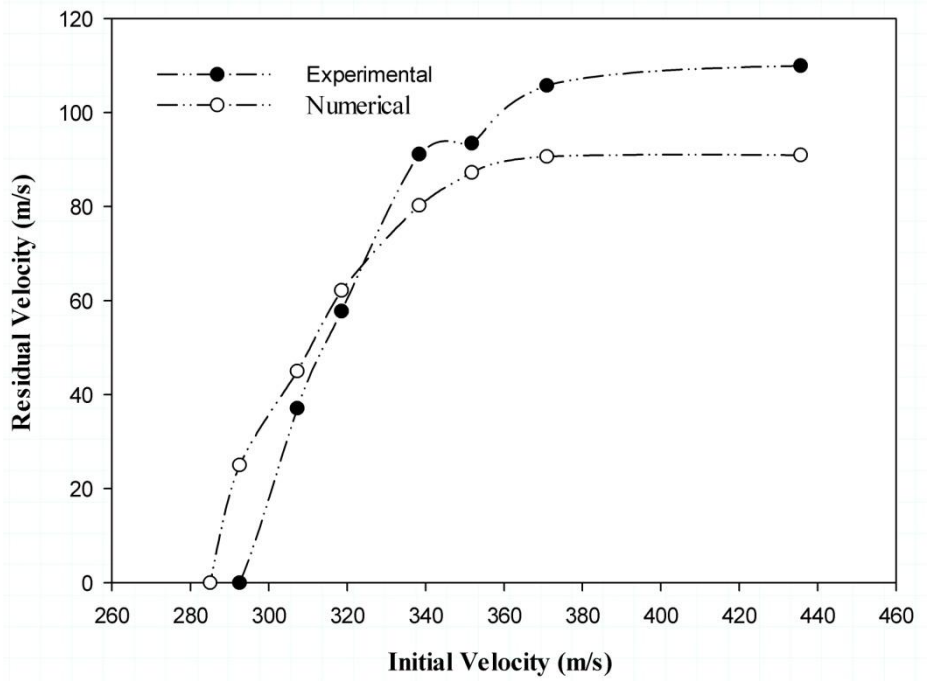

Figure 23 - Comparison of Experimental [3] & Numerical Solution for 20 mm Weldox 460E Target

6.2 Al 7075 T651

Following simulation results have been obtained for a 10 mm Al 7075 T651 target being impacted by a blunt projectile of Arne tool steel at a velocity of 500 m/s.

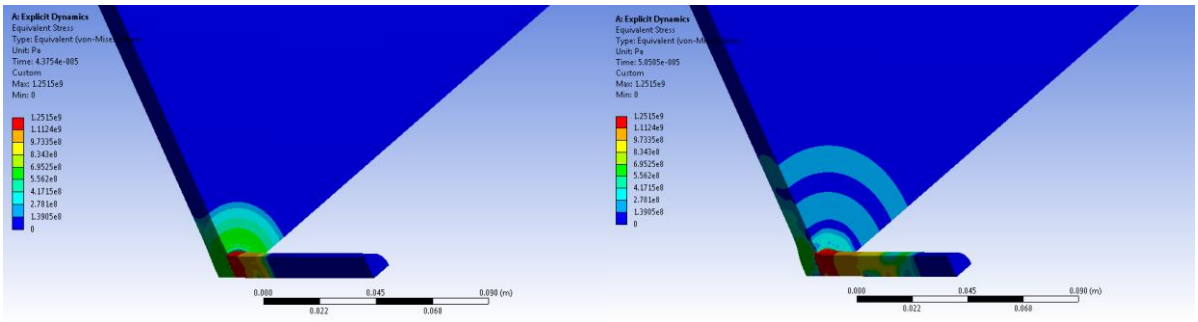

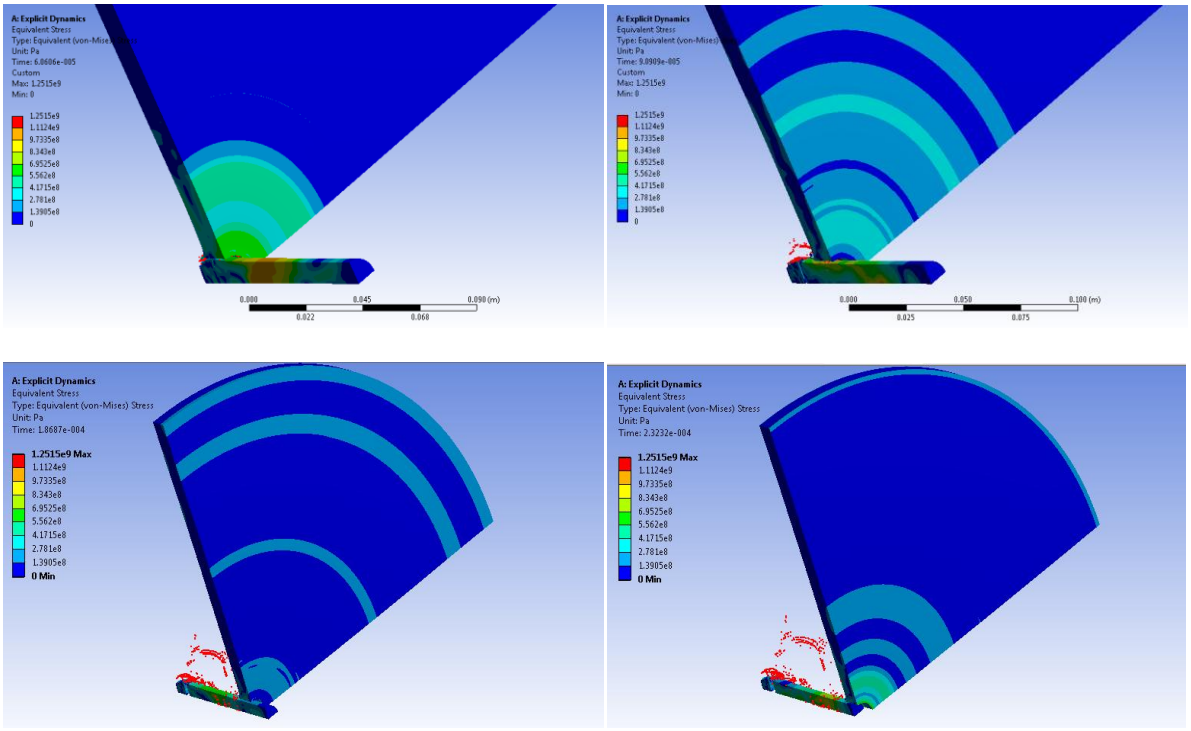

Figure 24 – Stress (Von-Mises) Contours at $t = 43.7, 50, 60.6, 90.9, 186$ & 232 μs

Al seems to mimic the failure mode of steel. A plug around the size of projectile diameter appears at the rear end of the target. High shear stress zones are formed around the periphery of projectile due to which the plug is practically sheared out of the target

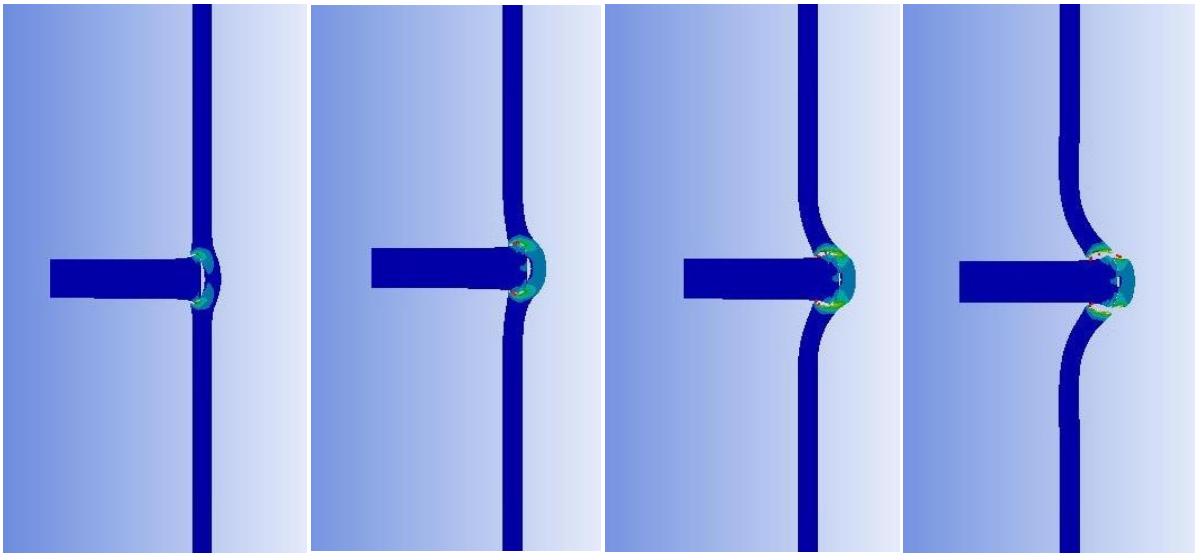

Figure 25 - Penetration at T= $43.7, 50, 60.6$ & 80.4 μs in AA 7075 T651

Following graph has been plotted for a blunt projectile impacting against a 20 mm AA 7075 T651 target.

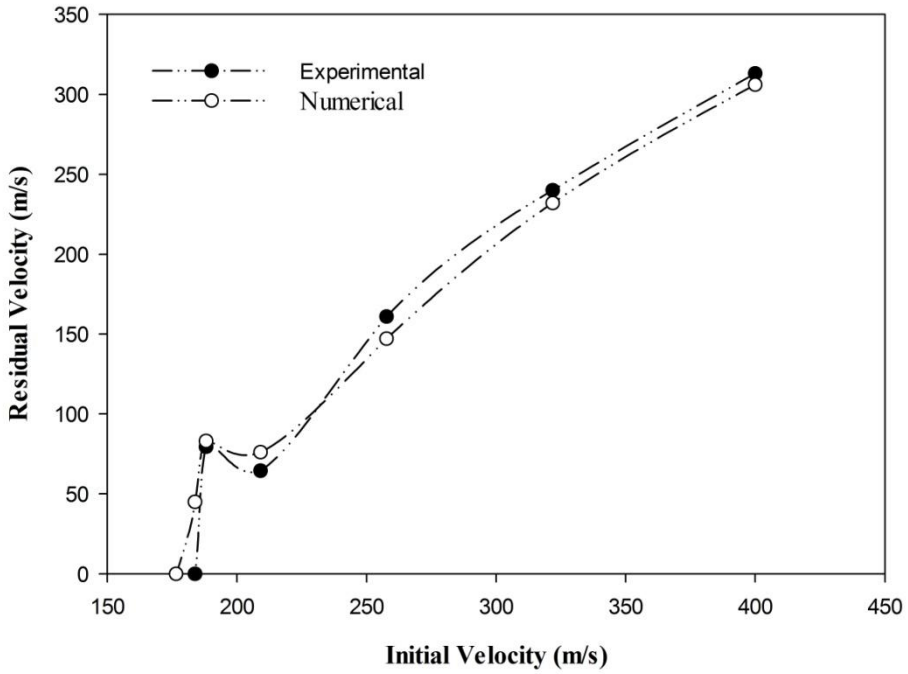

Figure 26 – Ballistic Limit Curve for 20 mm AA7075 Target

6.3 SiC

If the tensile strength of a material is lower than its compressive strength, then the initial compressive stress wave results in a radial fracture. This kind of failure can be observed in SiC-B as shown in the figure below. Residual velocity for SiC was found out to be 390 m/s.

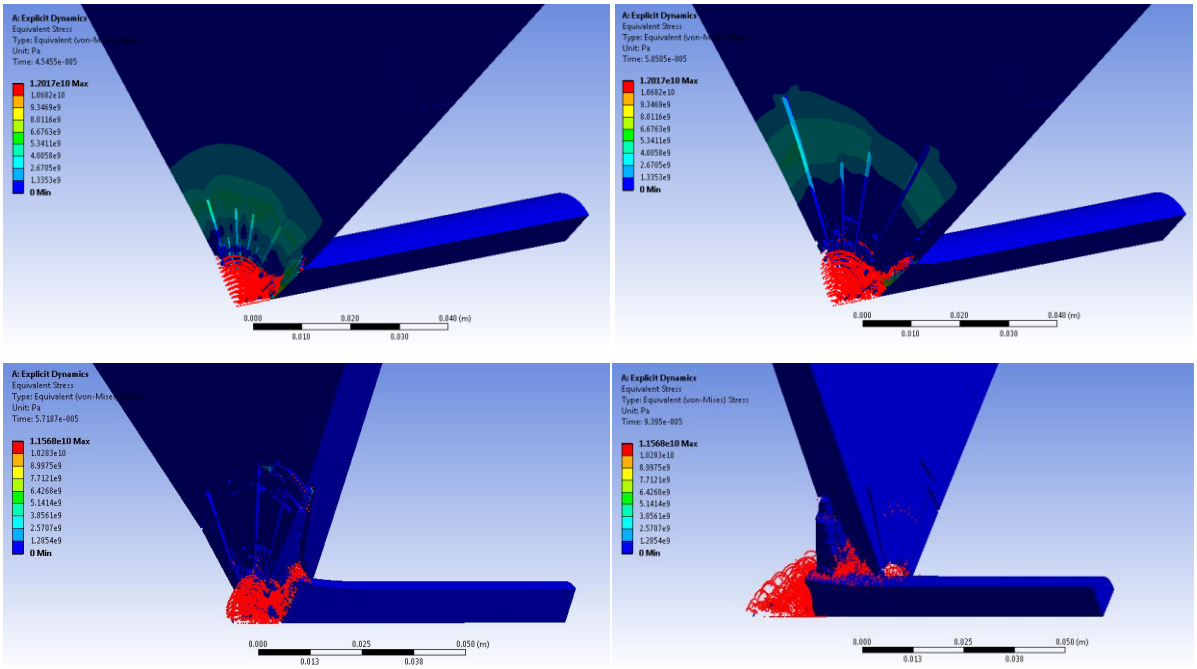

Figure 27 – Stress Contours at $t = 45.4, 50.5, 57$ & 93.9 μs

Damage can be observed on the rear surface of the target plate in the form of radial cracks. The material fails instantly upon impact without any signs of bulking. There is no sign of

plugging unlike metals. In fact, significant amount of pulverization can be observed in front of the projectile. Silicon Carbide fails due to high pressure induced pulverization. As shown above, damage on front side of the target is minimal as compared to the rear side, which shows how the failure in case of brittle materials. Damage initiates from the periphery of contact area of projectile and target.

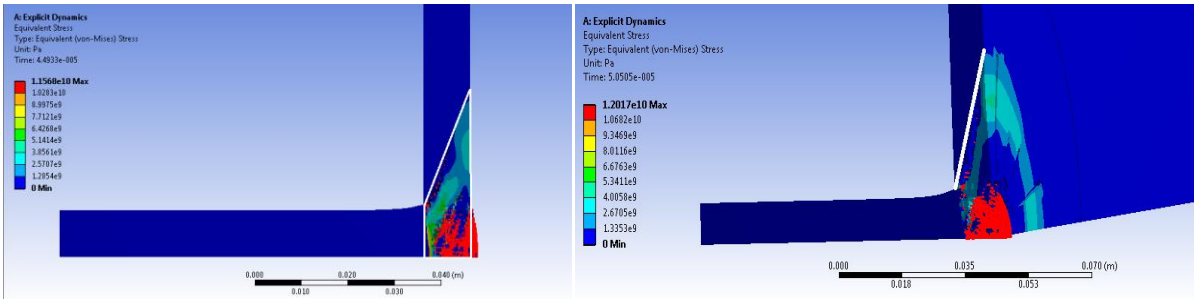

Figure 28 – Stress Wave Propagation Conoid in SiC

The conoid highlighted in white shows how the stress wave propagates as it moves in longitudinal as well as lateral direction. This is due to the fact that the initial compressive stress wave after reflection from the free end of target, resulted in a longitudinal wave causing the plate to fracture along the white line as shown above. The maximum tensile principal stress occured just outside the periphery of the contact region, and the resulting cone crack propagated towards the rear of the ceramic.

The angle of propagation of this wave is precisely 68.5°. The angle "68.5°" is the trajectory of minimum principal stress. This is merely due to the fact that by propagating along trajectories of minor principal stresses, cracks maintain orthogonality to the major component of tension, maximizing the strain energy release rate. Upper and lower cone diameters were measured to find the propagation angle for this wave. Although the condition of 68.5° was satisfied but it was observed that the crack propagation did not necessarily follow straight line but instead mimicked a semi-elliptical path. Minor to major axis ratio of this ellipsoid was approximately 0.32.

Another most important phenomenon associated with ceramics including SiC is the interface defeat phenomenon that is in other words the projectile deformation upon impact. Here is one of the simulation results physically depicting the kind of strain a blunt projectile undergoes. Flat ended projectile striking a target with high compressive strength resulted in significant projectile deformation in the form of mushrooming on the impact end.

Unlike metals, ceramics are in no way a standalone option to be used as monolithic targets but when used in combination with metallic sheets, ceramics play an enhanced role providing considerable ballistic resistance

6.4 CONICAL PROJECTILES AGAINST MONOLITHIC SHEET

Moving onto the conical projectiles, projectile with same material moving at a velocity of 400 m/s was used against a 20 mm Weldox target. Ductile hole enlargement was the dominant failure as evident in the figures given below, while petaling can be observed on the rear surface of the target. Residual velocity was calculated to be 315.42 m/s. Material in front of the projectile has been pushed away laterally.

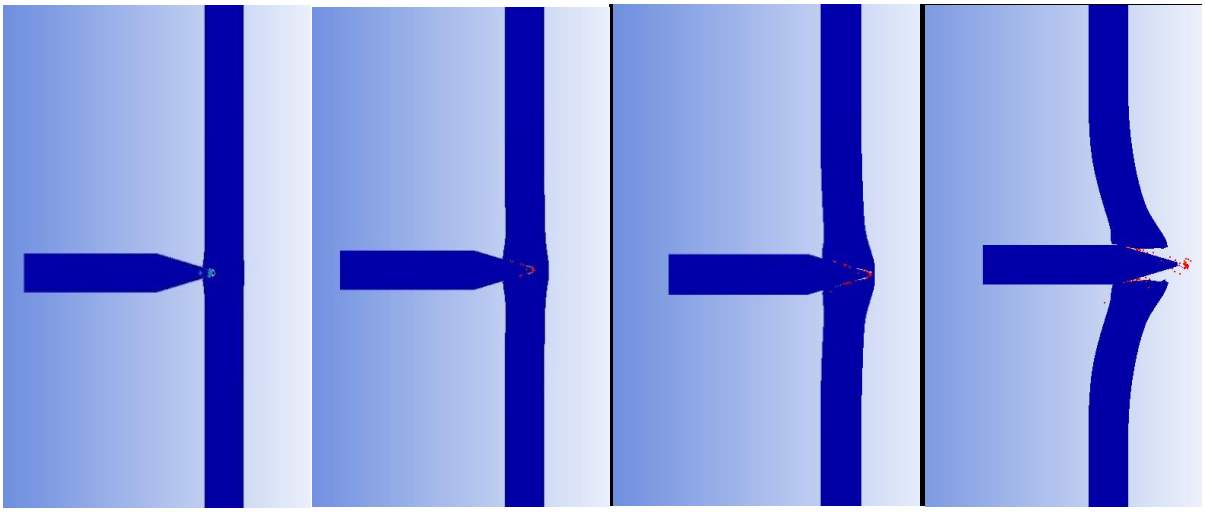

Figure 29 - Penetration at T= 64, 88, 115 & 189 µs in Weldox 460E

Following simulations have been performed with a conical projectile of 20 mm diameter impacting against a 12 mm thick Weldox 460E target sheet. Numerical results are quite comparable with the experimental results [35] but a significant difference can be observed as the impact velocity is reduced gradually. Numerically, the ballistic limit velocity was computed to be 258.4 m/s with a marked difference of 11.08 % from the experimental result of 290.6 m/s

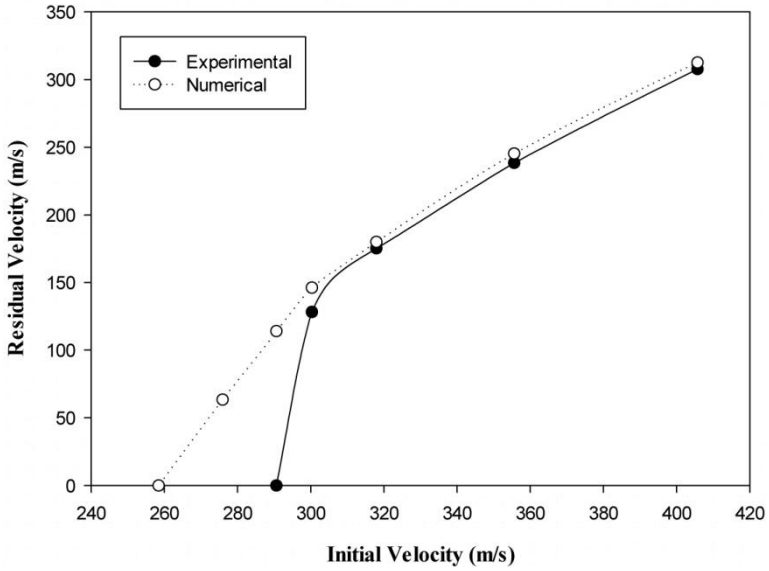

Figure 30 – Comparison of Experimental [35] & Numerical Results Weldox 460E

Another study was carried out to compare the residual velocities for blunt and conical projectiles. Numerical results were compared both for conical and blunt projectile impacting against a 12 mm target sheet. Simulation results show that the penetration capacity of blunt projectile is much more than conical nose projectile.

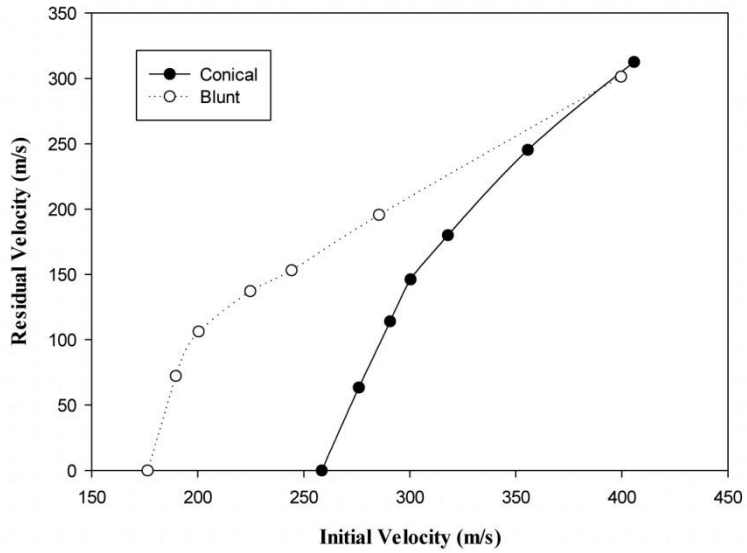

Figure 31 – Comparison of Conical and Blunt Projectiles

Comparing the numerical data for both kinds of projectile shapes, it was observed that Ballistic Limit velocity for conical projectiles was found to be higher than that of blunt projectiles. For in depth study of this problem, previous simulation results were recalled. As evident from the numerical simulations carried out for conical projectiles, target plate failed due to petaling which was a combination of shearing and bending. In case of blunt projectiles, plugging along with ductile hole enlargement was the dominant failure mode. Close analysis revealed that the major difference lied in the type of failure mode. More

energy was required for pushing the target material aside in case of conical projectile as compared to shearing a plug in case of blunt projectiles.

Below graph has been plotted for 12 mm thick conical plate

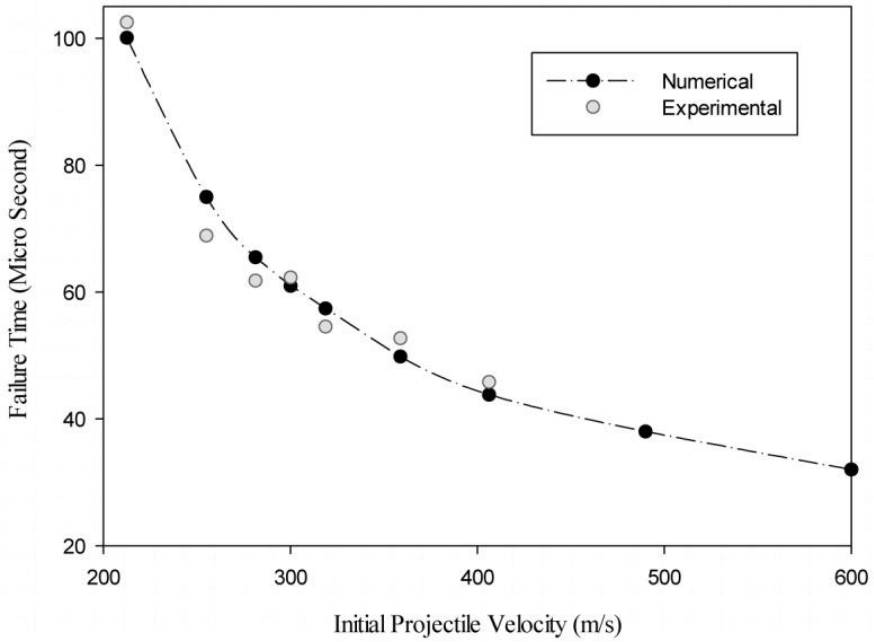

Figure 32 –Comparison of Numerical & Experimental results for Failure Time (Conical Projectile)

Same plot was developed for a blunt projectile impacting against a 12 mm thick target. Although the failure time did not necessarily follow the curve plotted as a result of regression analysis, but still a downward trend in failure time can be observed with the change in initial velocity. After 300 m/s, even a significant change in impact velocity didn't affect the failure time.

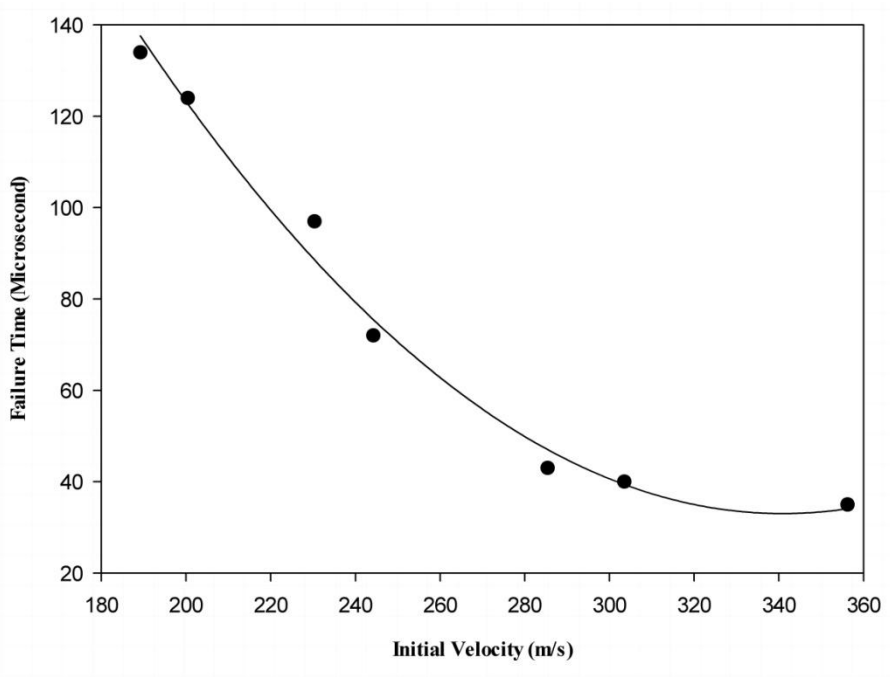

Figure 33 – Numerical Results for Failure Time (Blunt Projectile)

Comparison of above two graphs showed that for approximately equal velocities, conical projectiles tend to take more time to completely penetrate the target as compared to the blunt projectiles. For initial velocities of 303.5 m/s and 300 m/s, failure time equal to 40 μs and 61 μs was observed for blunt and conical projectiles respectively.

Following graph has been plotted for a conical projectile impacting against a 12 mm Weldox 460 E target at a velocity of 291 m/s.

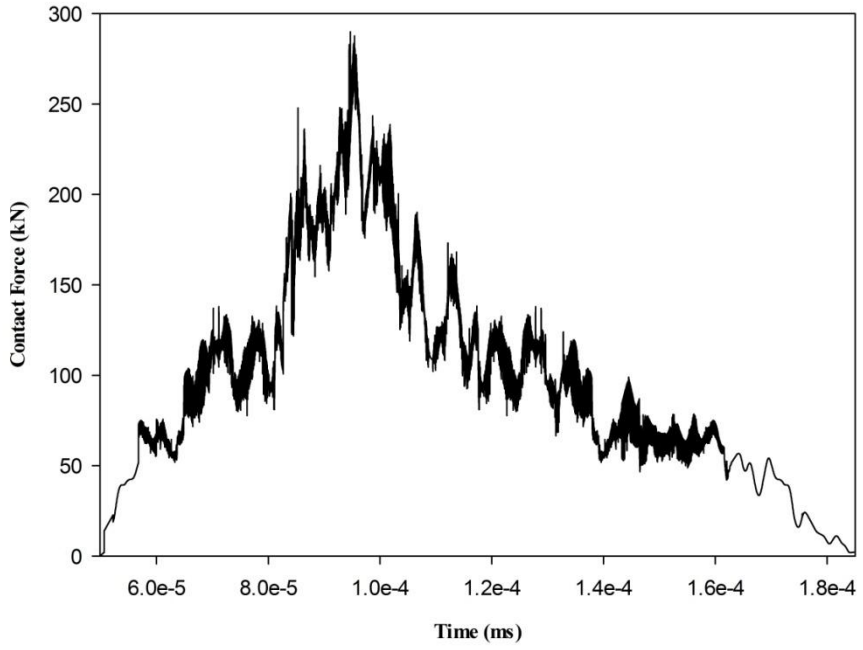

Figure 34 – Contact force Plot for Conical Projectile

Above graph showed that contact force increased up till 94.7 μs, which is exactly the same time at which the maximum number of nodes from both the target and projectile interacted with each other. At $t = 94.7\,\mu s$, the projectile was almost halfway through the target. Conical projectile didn't show much penetration capacity as compared to the blunt projectile. So, in case of Multi-Layered target, all simulations were carried out with Blunt projectile.

6.5 MULTI-LAYERED SHIELD

The study investigates the mechanisms of projectile arrest for fillings that span the disparate possibilities of high strength steel to very hard, but brittle ceramics, and examines the implications of these layering on both the panels ballistic limit and spatial extent of damage which influences multi-hit performance. The results were compared with those obtained for monolithic targets with the same range of target thickness.

Three very important properties are associated with ceramics that is low density, high compressive strength and hardness. Ceramics like Alumina and SiC are always used in combination with ductile materials aluminium usually. Ceramics due to their high compressive strength deform the projectile severely, at the same time reducing a significant amount of projectile's kinetic energy. This eroded and decelerated projectile is then easily stopped by the rear ductile plate. Hence the next optimum choice was double layered sheet with SiC as the front layer and Weldox 460E as the back plate.

Numerical results were obtained for a target of fixed thickness 12 mm with 2 mm air gap between the front and back layer.

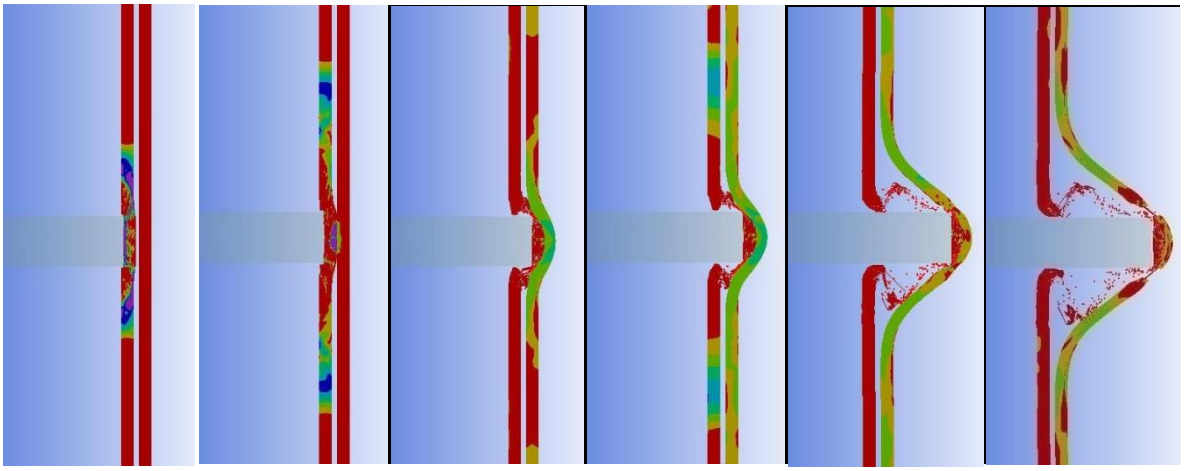

Figure 35 – Double-Layered Metallic Sheet SiC (Front) and Weldox (Back)

Equivalent Stress of the order of 7.86 GPa is developed in the front plate on impact with a maximum principal stress of 14.9 GPa. This principal stress is greater than the defined Hugoniot Elastic limit of 11.7 GPa for SiC. Therefore SiC fails instantly upon impact.

Much surprisingly, Silicon Carbide underwent considerable amount of plastic strain of around 3 before failure. It is evident that the front layer of silicon carbide undergoes much deformation during failure as compared to the back plate of Al7075. Silicon Carbide absorbs much of the impact force which is around 150 kN. This can be due to decrease in the thickness of SiC. Residual velocity of 373 m/s was observed in this case against an impact velocity of 400 m/s. Also the plastic work done by the ceramic layer on projectile was calculated to be 64 J which plastically deformed the impacting projectile. As expected, aluminium followed the same failure mode as observed in monolithic targets. Back plate eventually failed due to plugging.

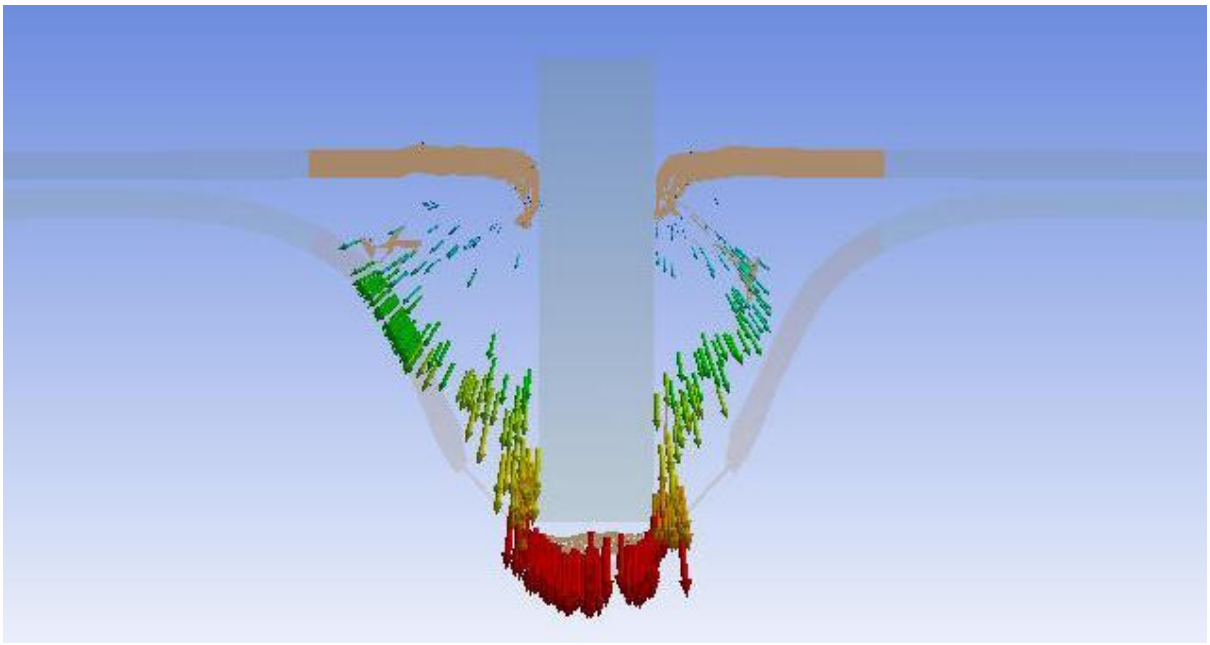

Figure 36 – Double-Layered Metallic Sheet SiC (Front) and Weldox (Back)

SiC fractures on impact as shown in the above figure. Downward arrows signify the distance covered by the eroded elements of SiC on impact. Maximum deformation of 6 mm was observed in the Weldox 460E plate.

The next obvious question was the relative thickness of two materials for a target of fixed size. So a study of optimum thickness ratio between the front and back layer was conducted. One widely used analytical model is the Florence model based on fracture cone formation

and energy dissipation in back plate. This model has been comprehensively studied by Ben Dor [21]. Another recent development was the introduction of an empirical model proposed by Ahmed Serjoui [42]. Optimum thickness ratio for Florence model was calculated and compared with the numerical results. A new parameter ξ was introduced for double layered targets, which was defined as

$$\xi = \frac{b_1}{b_2} = \frac{Thickness\ of\ Front\ Plate}{Thickness\ of\ Back\ Plate} \rightarrow (24)$$

Thickness ratio was increased from 0.5 up till 4 with equal increments of 0.5. Ballistic limit velocity results were obtained from the Florence model in each case. A simplified version of Florence model was computed putting all the required values and leaving the variables.

$$V_{bl} = \sqrt{\frac{(13.71 \times 10^8) b_2 (0.000314 + 12.56 b_1^2 + 0.1256 b_1)}{[(3227 b_1 + 2810 b_2)(0.000314 + 12.56 b_1^2 + 0.1256 b_1) + 0.197]}} \rightarrow (24)$$

Maximum thickness ratio value $\xi = 4$ resulted in high ballistic limit velocity equal 39.12 m/s as compared to the minimum thickness ratio value $\xi = 0.25$ which gave relatively low ballistic limit velocity equal to 38.06 m/s. While target plates with equal thickness resulted in a ballistic limit velocity of 44 m/s.

Numerical results were obtained for eight different values of ξ to reach an optimum solution as far as the thickness of two plates was concerned. Main idea was to find the shield which gave minimum residual velocity against an impact velocity of 400 m/s.

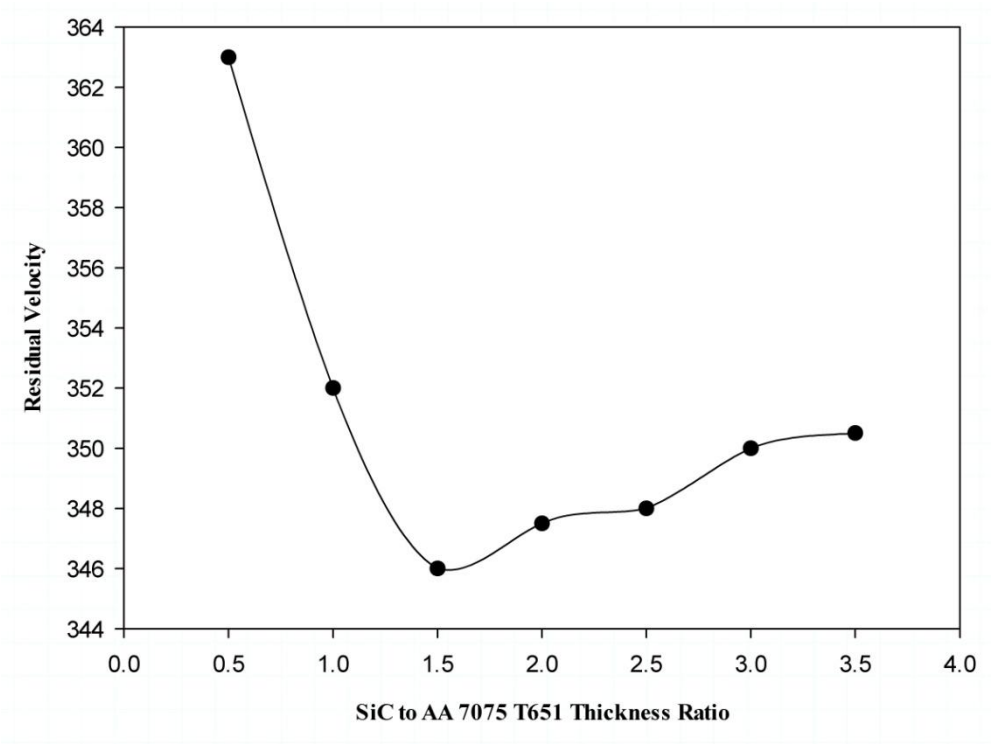

Figure 37 – Optimum Thickness Ratio

A steep decline in residual velocity was observed as the ceramic to metal thickness ration was increased to form 0.5 to 1.5. From 1.5 onward, a continuous increase in residual velocity was observed with no signs of improvement. So the ceramic to metal thickness ratio of 1.5 was adopted for final simulation, which gave the residual velocity of 346.3 m/s..

Now the next step was to test the blunt projectile moving at a velocity of 400 m/s against the combination of Al-SiC.

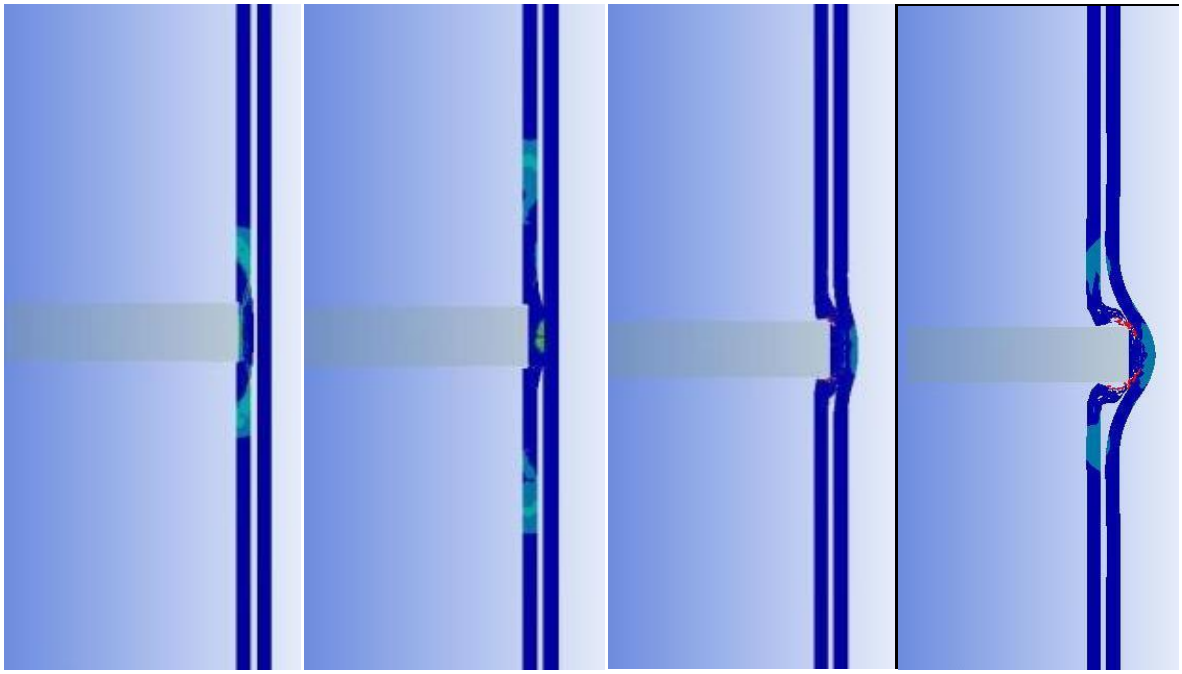

Figure 38 – Silicon Carbide Failure with SiC (Front) and Al (Back)

SiC followed the same failure pattern as observed in case of double layered SiC-Weldox target. Surprisingly, Aluminium didn't fail due to plugging but a longitudinal crack appeared as soon as the projectile hit the back plate. This represented a sort of tensile tearing in aluminium back plate.

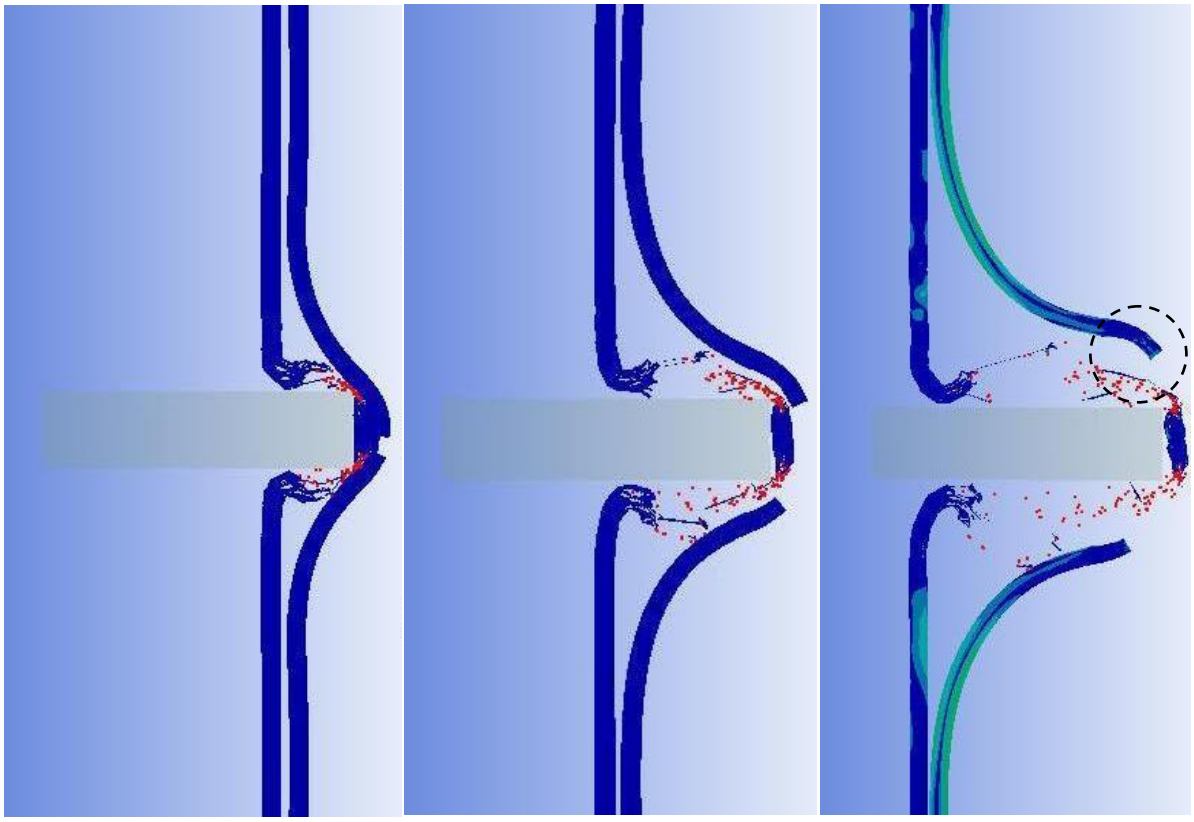

Figure 39- Al 7075 T651 Failure with SiC (Front) and Al (Back)

Finally, FEM simulation was run to test the blunt projectile moving at a velocity of 400 m/s, against an Al-Weldox target. The next critical decision was to either place aluminium or Weldox in front. Modified form of an analytical model proposed by Vitman [43] and Gabi Ben-Dor was used to find the optimum solution. Instead of defining the modeling parameters for a specific alloy, Vitman defined the materials in to a generic category as shown below. For this, a parameter χ was used which can be defined as the ratio of dynamical hardness and material density.

Table 4- Model Parameters [43]

Sr. No	Material	Dynamical Hardness (N/m^2)	Density (kg/m^3)	$\chi = \frac{Dynamical\ Hardness}{Density}$
1	Aluminium	350×10^6	2810	0.1245×10^6
2	Steel	1850×10^6	7850	0.2356×10^6

Gabi Ben-Dor [21] proposed that the plates, in multi-layered shields, must be arranged in increasing order of parameter χ for achieving maximum Ballistic Limit velocity. Two cases were run to check this proposition: one with Al in front and the second one with Weldox in front.

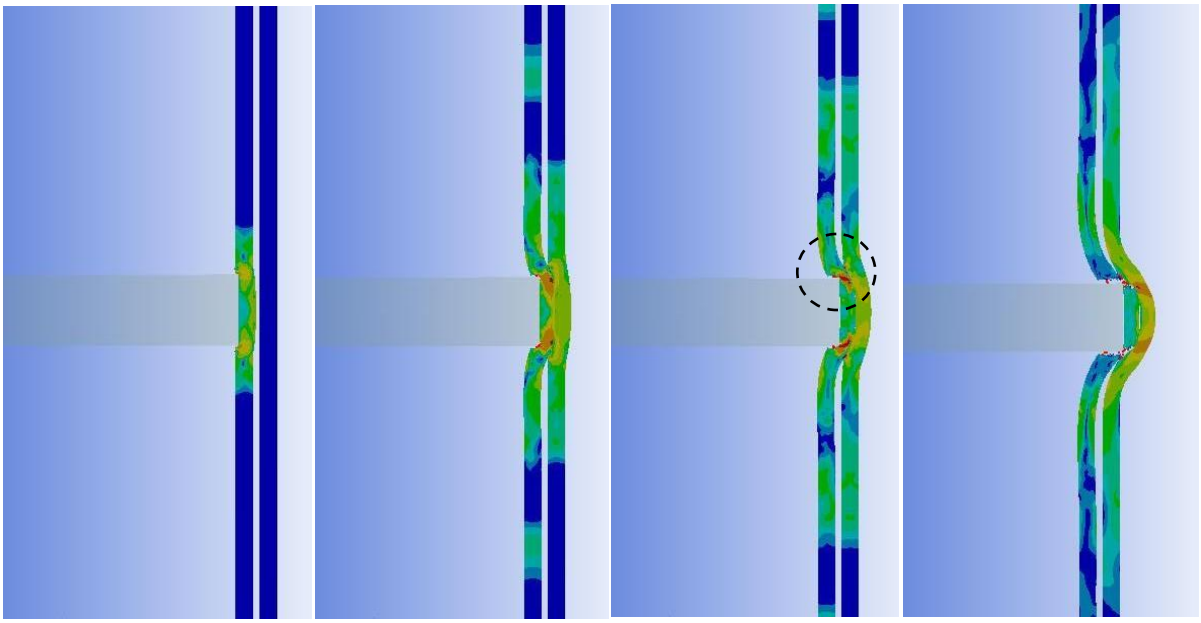

Figure 40 - Al 7075 T651 Failure with Al (Front) and Weldox (Back)

Very high shear stress of the order of 671 MPa was observed in the encircled region as evident in the above figure. Aluminium front plate failed due to the formation of these high

shear zones around the edges of impacting projectile. Both plates failed due to plugging.

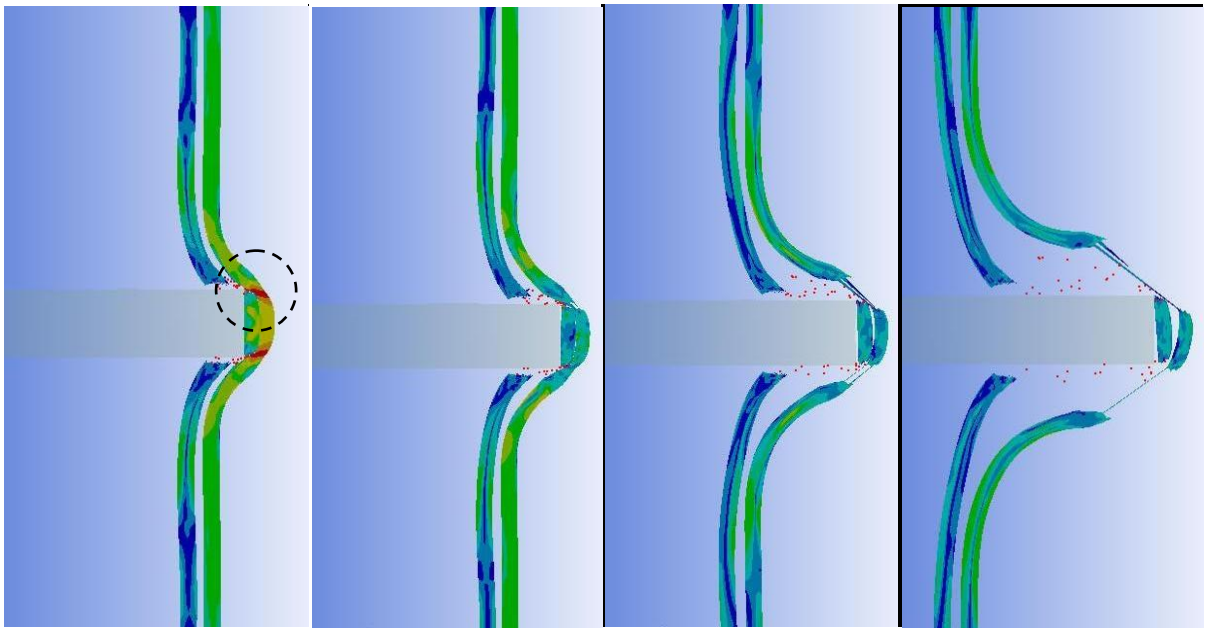

Figure 41 – Weldox 460E Failure with Al (Front) and Weldox (Back)

Same phenomenon was observed for Weldox back plate. Encircled area shows the formation of high shear stress zones of the order of 719 MPa. In the next phase, order of plates was reversed with Weldox in front and AA7075 T651 in back.

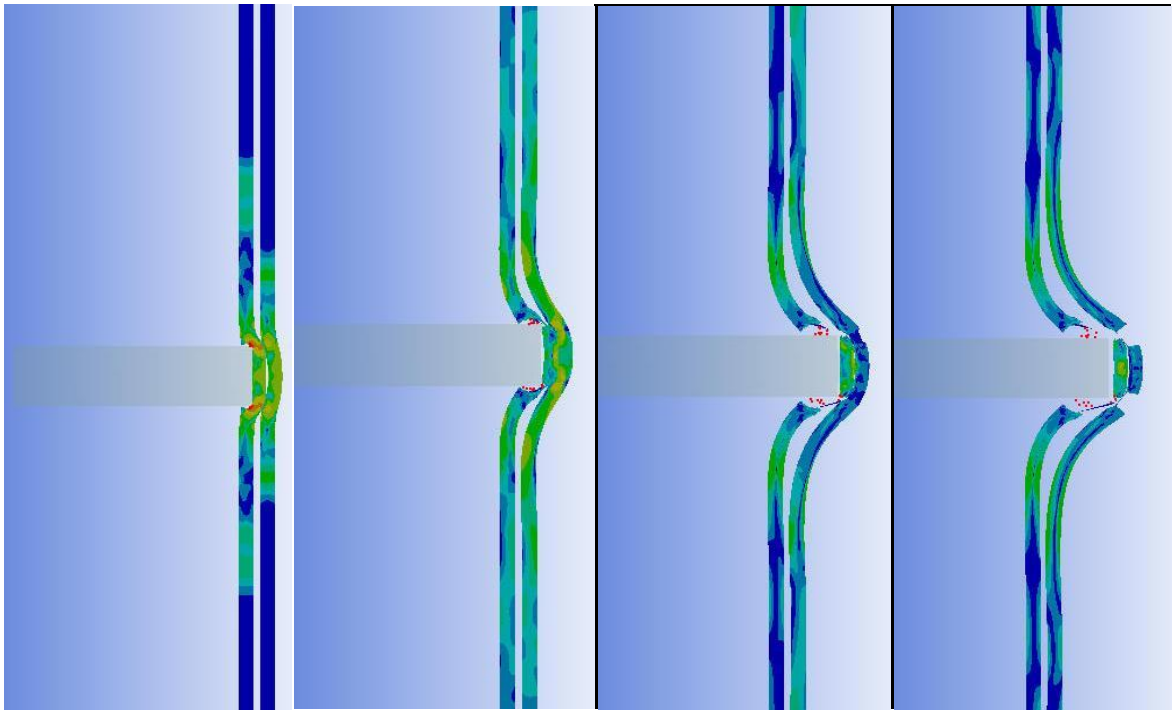

Figure 42 – Target Failure with Weldox (Front) and Al (Back)

Unlike the predictions from analytical solution proposed by Gabi Ben-Dor, multi-layered target with Weldox in front gave much less residual velocity for same initial velocity of 400

m/s. This result can be attributed to the fact that Weldox undergoes considerable strain before failure as compared to relatively less ductile AA 7075 T651.

Finally, results from all the numerical simulation were plotted to check the performance of each target type, against the blunt projectile for a fixed impact velocity of 400 m/s. Residual velocity gave a clear understanding of the Ballistic resistance of each target type. Weldox which is specifically manufactured as a Ballistic resistant shield gave minimum residual velocity of 326 m/s. While AA 7075 T651 gave maximum residual velocity of 382 m/s.

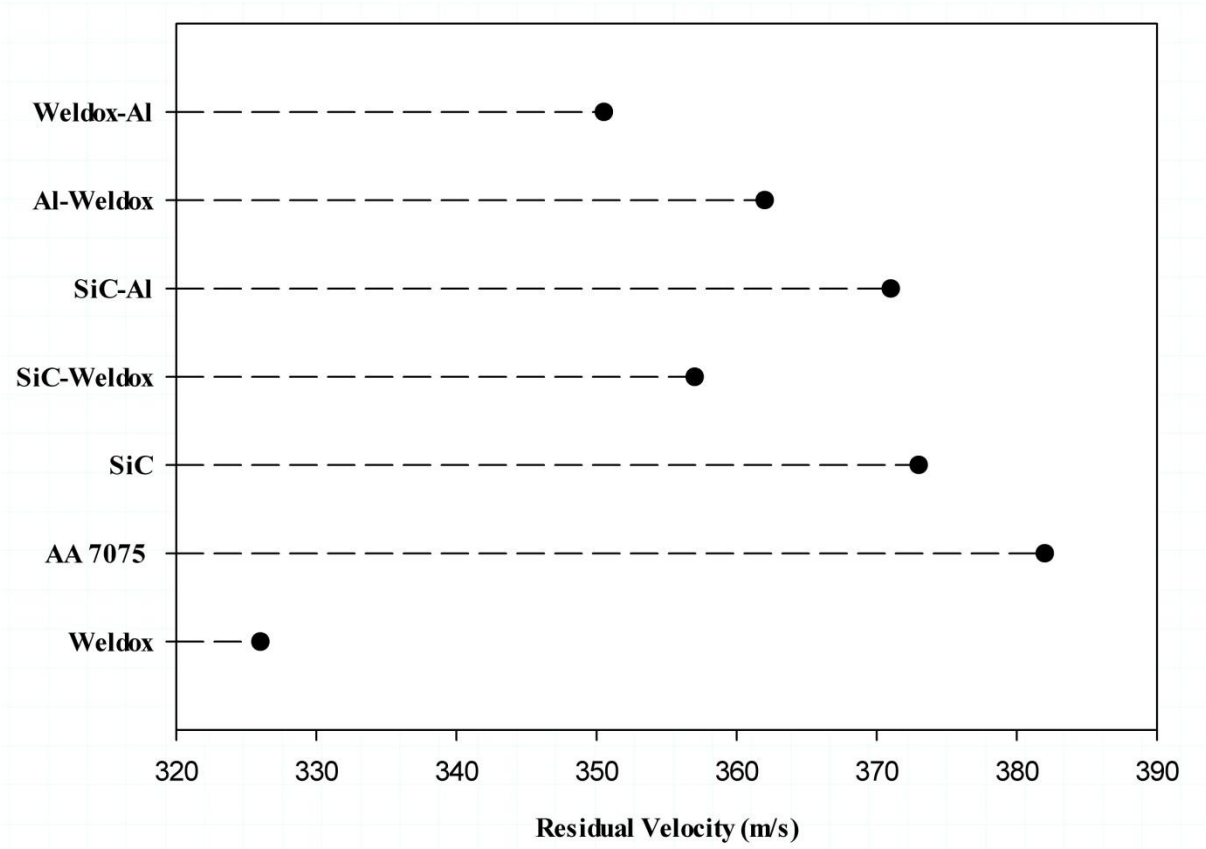

Figure 43 – Cumulative comparison of different target types

CHAPTER-7

7. CONCLUSION

Although light materials like Al7075 and SiC or any combination of them provides a good alternative to Weldox, which due to density has huge question mark on its future use as a monolithic shield, but still the level of ballistic protection provided by steel in general and Weldox in particular is unmatchable. The combination of Aluminium and SiC provides a good match with the ceramic significantly deforming the projectile and Al 7075T651 with its high ductility. Overall, the results obtained by explicit codes are comparable with the wide range of empirical data available in the literature.

Analytical techniques based on simplified or approximate assumptions lagged behind numerical results, as far as accuracy is concerned. However, analytical solutions using curve fitting based on empirical data provided remarkable results. In case of Weldox, analytical method overestimated the residual velocity as they were usually derived taking into account only a few material parameters neglecting some practically important ones. Metallic shields failed mainly due to plugging while ceramics failed due to radial fracture.

As far as the projectile shapes are concerned, simulations with blunt projectiles produce quite comparable results. Numerical accuracy of simulations with conical projectiles decreased drastically as the impact velocity was reduced.

CHAPTER-8

8. FUTURE WORK AND RECOMMENDATIONS

In order to qualify a ballistic resistant shield, it is tested against a range of projectiles moving at different velocities. This requires extensive experimental work which in turn needs sophisticated equipment & set up to capture impact and residual velocities. FEM simulations can help reduce the empirical work to minimum. Currently the Lagrangian based code give quite comparable results for moderate deformation. In case of large deformations, mesh free techniques like SPH or a combination of both FEM and SPH can be explored. SPH can be used in critical impact region coupled with FEM in far field. Modeling 7.62 mm projectile was the most difficult problem and realistic results could not be obtained in this phase. This work can be extended to estimate 7.62 mm projectile perforation against various target configurations.

9. REFERENCES

1. Jonas A. Zukas. “High Velocity Impact Dynamics”

2. T. Borvik et al. “Ballistic penetration and perforation of steel plates-an experimental and numerical investigation” Advances in Dynamics and Impact Mechanics-2000

3. T. Borvik et al. “Effect of target thickness in blunt projectile penetration of Weldox 460 E steel plates” International Journal of Impact Engineering 28 (2003) 413–464

4. Backman ME, Goldsmith W. “The mechanics of penetration of projectiles into targets” International Journal of Engineering Sciences 1987;16:1–99.

5. Yellup J. M. and R. L. Woodward, “Some investigation into the prevention of adiabatic shear failure in high strength armor materials” (1980) Res. Mech. pp 41-57

6. I. Marom and S. R. Bodner “Projectile perforation of multilayered beams” International Journal of Mechanical Sciences, 21(8):489 - 504, 1979.

7. J. Radin and W. Goldsmith. Normal projectile penetration and perforation of layered targets. International Journal of Impact Engineering, 7(2):229-259, 1988.

8. Curran et al. “Dynamic Failure in Solids” Physics Today” Physics Today, 30, 46-55, 1977

9. A. A. Almohandes, M. S. Abdel-Kader, and A. M. Eleiche. “Experimental investigation of the ballistic resistance of steel-fibreglass reinforced polyester laminated plates” Composites Part B-Engineering, 27(5):447-458, 1996.

10. S. Dey et al. “On the ballistic resistance of double-layered steel plates: An experimental and numerical investigation” 2006

11. V. S. Deshpande and N. A. Fleck, ‘‘One-Dimensional Response of Sandwich Plates to underwater Shock Loading,’’ J.Mech. Phys. Solids, 2347–83 (2005).

12. K. Nixdorff et al. “Application of the penetration theory of J. Awerbuch and S. R. Bodner on multilayered targets”, Math. Mech. 64:4 (1984), T147–T149.

13. J. W. Hutchinson and Z. Xue, ‘‘Metal Sandwich Plates Optimized for Pressure Impulses,’’ Int. J. Mech. Sci., 545–69 (2005).

14. Madhu et al. 2003 V. Madhu, T. B. Bhat, and N. K. Gupta, “Normal and oblique impacts of hard projectiles on single and layered plates: An experimental study”, Def. Sci. J. 53:2 (2003), 147–156.

15. J. A. Zukas and D. R. Scheffler, “Impact effects in multilayered plates”, Int. J. Solids Struct. 38:19 (2001), 3321–3328.

16. Ben-Dor et al. 1998a] G. Ben-Dor, A. Dubinsky, and T. Elperin, “Effect of air gaps on ballistic resistance of targets for conical impactors”, Theor. Appl. Fract. Mech. 30:3 (1998), 243–249.

17. Ben-Dor et al. 1998b] G. Ben-Dor, A. Dubinsky, and T. Elperin, “On the ballistic resistance of multi-layered targets with air gaps”, Int. J. Solids Struct. 35:23 (1998).

18. G. Ben-Dor., A. Dubinsky, and T. Elperin, “Effect of air gap and order of plates on ballistic resistance of two layered armor”, Theor. Appl. Fract. Mech. 31:3 (1999), 233–241.

19. Ben-Dor. et al. “The optimum arrangement of the plates in a multilayered shield”, Int. J. Solids Struct. 37:4 (2000), 687–696.

20. Ben-Dor. et al. 2005 “Ballistic impact: Recent advances in analytical modeling of plate penetration dynamics”, Appl. Mech. Rev. 58:6 (2005), 355–371. A review.

21. Ben-Dor. et al. “Applied high-speed plate penetration dynamics, Solid State and its Applications 132, Springer, Dordrecht, 2006.

22. Ben-Dor. et al., “Effect of air gaps on ballistic resistance of ductile shields perforated by non-conical impactors”, J. Mech. Mater. Struct. 1 (2006), 279–299.

23. Ben-Dor. et al., “Applied High Speed Plate Penetration Dynamics” 2006

24. Christian J. Yungwirth et al., “Explorations of Hybrid Sandwich Panel Concepts for Projectile Impact Mitigation” J. Am. Ceram. Soc., S62–S75 (2011)

25. D.S. Preece, V.S. Berg, “Bullet impact on steel and Kevlar/steel armor-Computer modeling and experimental data” Proceedings of ASME symposium, July 25-29, 2004

26. S. Swaddiwudhipong et al. “High Velocity Penetration/Perforation Using Coupled Smooth Particle Hydrodynamics-Finite Element Method” International Journal of Protective Structures – Volume 1 · Number 4 · 2010

27. Jonas A. Zukas et al., “Practical Aspects of Numerical Simulations of Dynamic Events: Effects of Meshing” International Journal of Impact Engineering-2000

28. T.J. Holmquist and G.R. Johnson, “Determination of constants and comparison of results for various constitutive models” Journal De Physique III, Vol. 1, Oct. 1991, pp. 853-860.

29. Stefan Hiermaier, “Structures under Crash and Impact-Continuum Mechanics, Discretization and Experimental Characterization” Edition-2007.

30. Charles E. Andrson Jr. “A review of Computational ceramic Armor Modelling” Advances in Ceramic Armor-II

31. Yueming Liang et al. “Design and Simulation of Ballistic resistant Metal/Ceramic sandwich structures” Advances in Ceramic Armor-2005, pp 35-42.

32. Chen, X. W., and Li, Q. M., 2003, “Perforation of a Thick Plate by Rigid Projectiles,” Int. J. Impact Eng, pp. 743–759.

33. Johnson, W., “Impact Strength of Materials” London, Arnold, 1972 [pp. 342, 360, 361,366].

34. P. Lundberg et al. “Impact of conical tungsten projectiles on flat Silicon carbide targets: Transition from interface defeat to penetration” Int. J. of Impact Engineering 28 (2006) pp:1842-1856

35. T. Borvik et al. “Perforation of 12 mm thick steel plates by 20 mm Diameter projectiles with flat hemispherical and conical noses” Int. J. of Impact Engineering 2002;27(1):19 35.

36. ANSYS Help Manual

37. Dey S., High strength steel plates subjected to projectile impact – An experimental and numerical study” Doctoral Thesis, Norwegian University of Science and Technology, 2004

38. Forrestal M. J. et al. “Penetration of 6061 T651 aluminium targets with rigid long rods” Journal of Applied Mechanics 1988, 55, 755-760

39. Ravid M. et al. “Dynamic perforation of viscoplastic plates by rigid projectiles” International Journal of Engineering Science 1983, 21, 577-591

40. Borvik et al. “Numerical simulation of plugging failure in Ballistic penetration” International Journal of Solid structures 2001, 38, 6241-64

41. Chen et al. “On perforation of ductile metallic plates by blunt rigid projectile” European Journal of Mechanics A/Solids 2009, 28,273-283

42. Ahmad Serjoui et al. “An empirical model for ballistic limit of bi-layer ceramic/metal armour” Procedia Engineering 75 (2014) 14-18

43. Vitman at al. “ A simple method of determining the dynamical hardness of metals using a double cone” Zavodskaja Laboratorjia 14(6), 727-732